Avian MRP126 Restricts Microbial Growth through Ca(II)-dependent Zn(II) Sequestration

Aaron T. Bozzi and Elizabeth M. Nolan*

Department of Chemistry, Massachusetts Institute of Technology, Cambridge, Massachusetts 02139, United States

*Corresponding author: lnolan@mit.edu

Phone: 617-452-2495

Abstract

The calgranulins form a class of S100 proteins in higher vertebrates that innate-immune cells release in abundance at infection sites. These proteins function by binding transition metal ions to prevent microbial pathogens from obtaining those essential nutrients. Mammals express three distinct members of this family, S100A8 (calgranulin A), S100A9 (calgranulin B, which heterooligomerizes with S100A8 to form calprotectin), and S100A12 (calgranulin C), that exhibit Ca(II)-dependent transition-metal-binding properties. Human calprotectin effectively sequesters Mn(II), Fe(II), Ni(II), and Zn(II), whereas human S100A12 selectivity sequesters Zn(II) over these other metal ions. Birds and reptiles express a single calgranulin homolog named MRP126, which we reasoned could have properties more similar to either calprotectin or S100A12. Here we present the purification and biophysical characterization of chicken MRP126 and, to the best of our knowledge, provide the first assessment of the metal-binding and antimicrobial properties of an avian MRP126. We show that MRP126 is a homodimer that selectively sequesters Zn(II) and restricts the growth of certain microbes. MRP126 binds Zn(II) at two canonical His_3Asp sites. The presence of excess Ca(II) increases the affinity of the His_3Asp sites from the low-nanomolar to the low-picomolar range, thereby enhancing antimicrobial activity. Chicken MRP126 also binds additional Zn(II) equivalents with low-nanomolar affinity at two non-conserved dicysteine sites and with high-nanomolar affinity using a histidine-rich C-terminal tail that is a hallmark of this clade of calgranulins. Our results with chicken MRP126 suggest that Ca(II)-dependent Zn(II) sequestration was a role of the last common ancestor of calgranulin proteins, with mammalian calprotectin subsequently evolving a broader metal-binding repertoire.

For Table of Contents Only

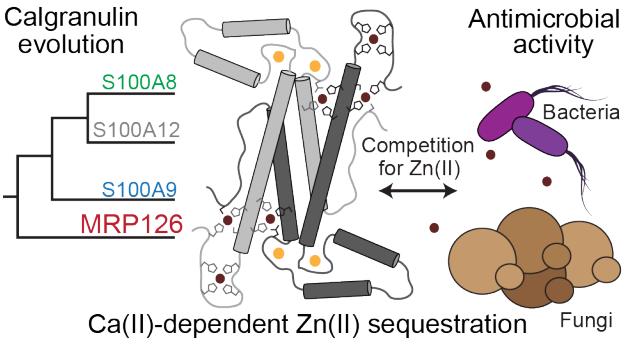

Introduction

The S100 protein family comprises numerous small (10–15 kDa) α-helical proteins, typically found as dimers, that use EF-hand motifs to bind Ca(II).[1] Specific to chordates, S100 proteins fulfill a variety of biological functions, including intracellular regulatory roles and extracellular cell-to-cell signaling that leverage the ability of these proteins to sense Ca(II).[2, 3] The calgranulins, which form a subgroup of the S100 family, include the mammalian homologs S100A8 (calgranulin A, also known as myeloid-related protein (MRP) 8), S100A9 (calgranulin B, MRP14), and S100A12 (calgranulin C).[4] The S100A8 and S100A9 polypeptides can heterodimerize and -tetramerize to form calprotectin (CP).[5] Many bird and reptile species possess a single calgranulin homolog named MRP126.[6] These proteins likely all diverged from a single protein present in the last common ancestor of higher vertebrates, although the precise order of gene duplication and speciation leading to the current distribution of homologs remains uncertain.[6]

Calgranulins are abundantly expressed in and secreted by white blood cells, especially neutrophils, where they contribute to the innate-immune response to infection.[7, 8] One conserved function involves the activation of pro-inflammatory signaling pathways and thus the recruitment of additional innate-immune cells to infection sites.[9-12] For example, S100A12 and CP (as well as S100A8 and S100A9 homodimers) have been reported to activate Toll-like receptor 4 (TLR4)[13-15] and the receptor for advanced glycation end products (RAGE)[15-18] to ultimately stimulate cytokine production.

As a second important function, calgranulins inhibit the growth of microbial pathogens by restricting the availability of essential transition metal nutrients as part of the innate-immune system's strategy of "nutritional immunity."[5, 19-23] Studies with human (hCP) and murine (mCP) homologs of CP demonstrated its ability to bind numerous divalent first-row transition metal ions (including Mn, Fe, Ni, and Zn) with high affinity and thereby starve pathogens of those essential nutrients.[24-31] This versatility depends on a biologically unprecedented hexahistidine (His_6) metal-binding site formed at the heterodimer interface.[26-28, 30, 32, 33] CP also contains a second high-affinity metal-binding site comprised of three histidines and an aspartate (His_3Asp) that sequesters Zn(II) but not Mn(II), Fe(II) and Ni(II).[25, 28, 29, 30] The S100A12 homodimer contains two His_3Asp metal-binding sites[34, 35] that provide Zn(II)-selective metal sequestration.[36] Because of its ability to sequester multiple nutrient metal ions, CP restricts the growth of a broader range of microbes than does S100A12.[24, 25, 28, 36]

Studies of CP and S100A12 show that Ca(II) ions play an important role in the behavior of these proteins. In particular, coordination of Ca(II) ions to the EF-hand domains enhances the metal-binding affinities and antimicrobial activity of both CP and S100A12. These observations form the basis of a model where physiological extracellular concentrations (≈2 mM) of Ca(II) increase the affinity of CP and S100A12 for transition metal ions[25, 29, 33, 37] and thereby improve their antimicrobial potency.[25, 28, 36] For CP, Ca(II) binding at the EF-hands or transition-metal binding at the His_6 site also causes two heterodimers to dimerize, thus forming a heterotetramer.[25, 38, 39] The Ca(II) concentration required for tetramerization varies between mCP and hCP, with a significantly higher amount needed for mCP.[40] For S100A12, higher-order oligomerization states have also been observed in the presence of Zn(II) (tetramers) and Zn(II) and Ca(II) (higher-order oligomers, which may include tetramers or hexamers).[41, 42]

To improve our understanding of calgranulin evolution, we aimed to evaluate the biochemical, biophysical properties, transition-metal binding ability, and antimicrobial activity of a bird or reptile MRP126 and thereby help establish the biological role of that branch of the calgranulin clade. As birds and reptiles typically have only a single calgranulin homolog, we reasoned that MRP126 likely functions analogously to either mammalian CP or S100A12.

We selected chicken MRP126 for this work because previous *in vivo* studies suggested it had a role in the chicken innate-immune response to bacterial infection. In particular, MRP126 was found to be highly abundant in splenic heterophils (the functional equivalents of neutrophils in birds) and macrophages.[43-45] In addition, *MRP126* RNA and MRP126 protein expression increased 40- and 300-fold, respectively, in the chicken cecum following oral infection with *Salmonella enterica* serovar Enteritidis.[44, 46] Inoculation of chicks with adult chicken microbiota also stimulated MRP126 expression in the cecum.[47] Although we are unaware of any direct evidence to date demonstrating an antimicrobial function for MRP126, these findings are consistent with MRP126 performing a similar innate-immune function to that of mammalian CP and/or S100A12. Moreover, chicken MRP126 was previously purified from *Escherichia coli* using a polyhistidine affinity tag[6] and shown to stimulate chicken TLR4 to activate NF-κB, suggesting a conservation of a pro-inflammatory signaling role within the calgranulin family.[6]

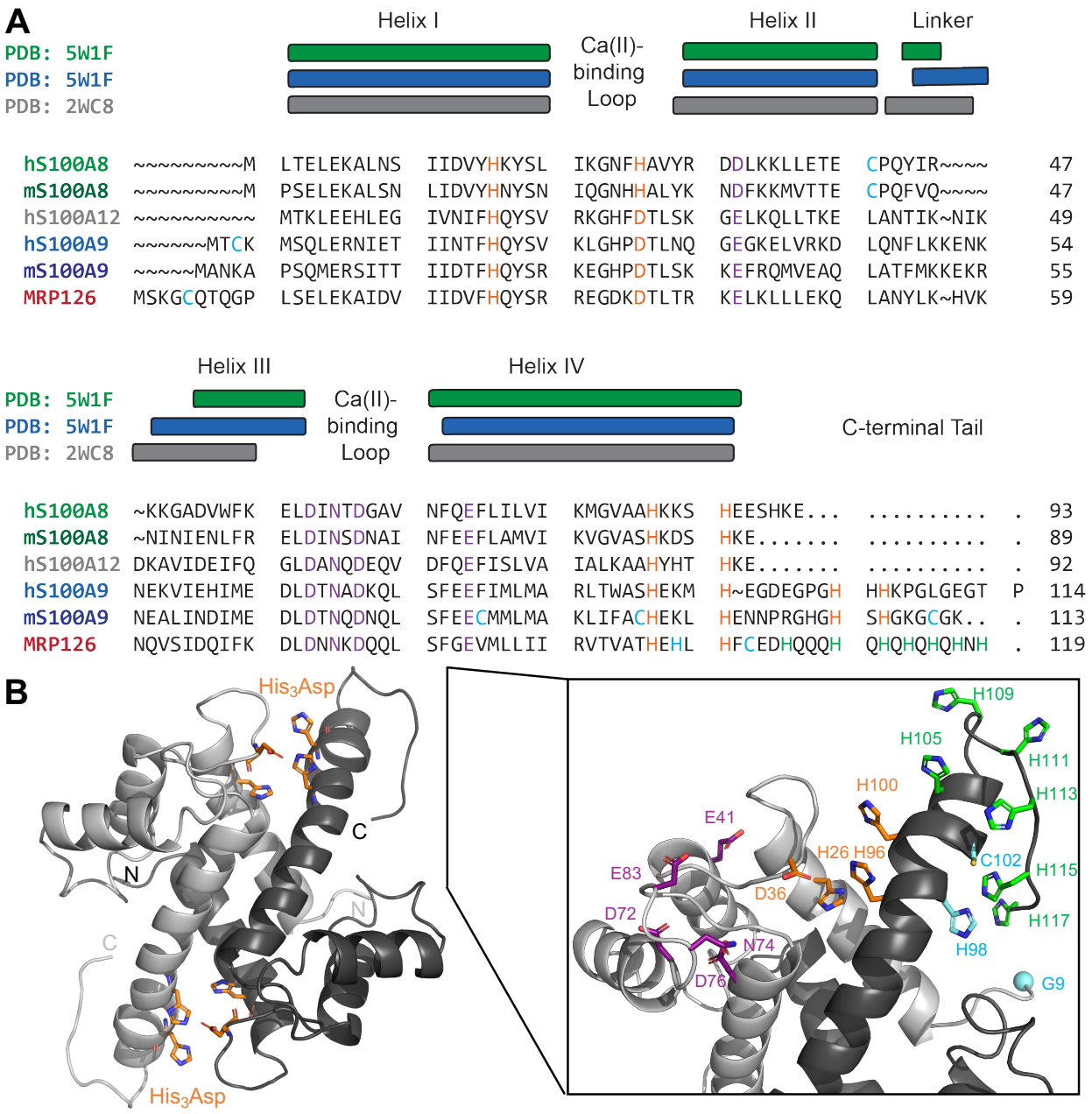

Figure 1: MRP126 is an avian homolog of mammalian S100A8, S100A9, and S100A12. (**A**) Sequence alignment of human (h) and mouse (m) S100A8, S100A9, human S100A12, and chicken (c) MRP126. The locations of the helices seen in calprotectin (PDB: 5W1F[30]) and S100A12 crystal structures (PDB: 2WC8[35]) are indicated above the alignment. Known/expected transition-metal-binding residues are highlighted in orange, Ca(II)-binding residues are purple, all cysteines as well as H98 in MRP126 are cyan, and the seven C-terminal tail histidine residues in MRP126 are green. (**B**) Homology model of homodimeric MRP126 generated with SWISS-MODEL[48] using an NMR solution structure of the Ca(II)-bound human S100A9 homodimer as the template (PDB: 5I8N[49]). The predicted His_3Asp sites are highlighted in orange in the left panel and the N- and C-termini of each monomer are indicated. In the right panel, a zoomed-in view of the top half of the homology model includes side chains for the residues highlighted in the sequence alignment (same color code) as well as a cyan sphere for the position of N-terminal residue (G9), which we highlight because C5 precedes this position and thus is not included in the model. See also Figure S1 for a sequence logo generated from 118 avian/reptile MRP126 homologs.

From sequence comparisons of chicken MRP126 to mammalian S100A8, S100A9, and S100A12 proteins (Figure 1A), each chicken MRP126 monomer contains two Ca(II)-binding EF-hand motifs. Each MRP126 homodimer likely possesses two transition-metal-binding sites at the dimer interface, as the three histidine and aspartate residues that form the His_3Asp site in CP and S100A12 are present in MRP126. In addition, chicken MRP126 has a histidine-rich C-terminal tail, a common feature of avian/reptile calgranulin homologs (Figure S1). We hypothesized this tail could allow MRP126 to form a six-coordinate metal-binding site analogous to the His_6 site of CP, which includes four histidine residues from the S100A8/S100A9 interface (His_4 site) and two histidine residues from the C-terminal tail of S100A9. To further explore potential MRP126 metal-binding sites, we generated a homology model (Figure 1B) of the protein with SWISS-MODEL[48] using an NMR solution structure of the Ca(II)-bound human S100A9 homodimer as the template (PDB: 5I8N).[49] From this structural model, it appears likely that in MRP126, His26, Asp36, His96, and His100 form two His_3Asp metal-binding sites at the dimer interface, whereas the histidine-rich C-terminal tail (containing His105, His109, His111, His113, His115, His117, and His119) could either contribute additional ligands to these sites or form separate metal-binding sites, perhaps also including His98 and Cys102. In this work, we aimed to test these hypotheses and assess how the functional properties of MRP126 compare to previously-studied mammalian calgranulins.

Here we present the purification and characterization of chicken MRP126. We show that MRP126 is an α-helical homodimer that sequesters Zn(II) and exhibits similar antimicrobial properties to human S100A12. MRP126 fulfils this role by binding two equivalents Zn(II) at the conserved His_3Asp sites with Ca(II)-dependent affinities. MRP126 also binds additional equivalents of Zn(II) with lower affinity at non-conserved sites involving two cysteines and its histidine-rich C-terminal tail. These results suggest that Zn(II) sequestration is the ancestral role in this clade of the S100 family, with mammalian CP likely developing the broader metal-withholding repertoire that underlies its more potent antimicrobial ability after the evolutionary split between the ancestors of modern mammals and those of birds and reptiles.

Materials and Methods

Complete experimental details are provided as Supporting Information.

Results

Purification and characterization of chicken MRP126 and variants. Guided by our prior work with mammalian S100 proteins,[25, 32, 36, 40, 50] we overexpressed MRP126 in *E. coli* from a codon-optimized gene inserted into pET41a. SDS-PAGE analysis showed that the expressed protein was soluble, and that overnight expression at 25 °C after induction with 0.5 mM IPTG maximized protein production. Starting from a cell pellet obtained from 2 L of culture, we combined the soluble fractions from two rounds of sonication and centrifugation and added 50% ammonium sulfate to precipitate contaminating proteins. The protein was subsequently dialyzed and purified using cation exchange chromatography and size-exclusion chromatography (SEC). The pure protein was then dialyzed against Chelex resin to remove contaminating metal ions. Typical yields of MRP126 were ≈60–90 mg / 2 L of culture.

For interrogating predicted metal-binding residues, we also designed and purified several variants of MRP126. We used site-directed mutagenesis to make the quadruple mutant ΔHis$_3$Asp (H26N/D36S/H96N/H100N), in which the four conserved metal-binding residues in the putative His$_3$Asp site are replaced with shorter hydrophilic residues. This variant was less stable than the native protein and we therefore reduced the ammonium sulfate concentration to 20% during the precipitation step and added 75 mM NaCl during the subsequent dialysis steps to keep it soluble during purification. We also generated a truncated variant of MRP126 named ΔTail in which the histidine-rich tail was removed by replacing the codon encoding H105, the first of the seven histidine residues in the C-terminal tail, with a stop codon. We also generated three more single-point mutants: C5S and C102S, each missing one of the two native cysteines that could contribute to a non-canonical (among the calgranulins) metal-binding site, and D36H, in which the putative metal-binding site aspartate is replaced with a histidine to create a potential His$_4$ site similar to the one found in CP (or His$_6$ site if tail histidine residues also contribute). These variants were expressed and purified analogously to the native protein except that the ΔTail variant required a different salt gradient for cation exchange chromatography. Typical yields for these variants were 60–100% of that for native MRP126.

Native MRP126 and all variants were produced in high purity as determined by SDS-PAGE (Figure S2). Mass spectrometry of the purified proteins indicated that MRP126 and all variants had the expected molecular weights for the species lacking the N-terminal methionine, a common post-translational

modification in *E. coli* (Table S2). ICP-MS analysis confirmed that the purified proteins were obtained in the apo form with only trace amounts of contaminating transition metal ions (Table S3).

Chicken MRP126 is an α-helical homodimer. Circular dichroism spectroscopy indicated a predominantly α-helical secondary structure for MRP126 and variants (Figure S3) with negligible change upon Ca(II) addition, as expected based on the structures of other S100 proteins. In a thermal denaturation assay in which the molar ellipticity was monitored at 226 nm as the temperature was increased from 35 °C to 95 °C in 1-°C intervals (Figure S4), we detected an apparent melting temperature (T_m) of ≈81 °C for MRP126 (8 μM) in both the absence and presence of 2 mM Ca(II). Thus, in contrast to previous studies of CP and mCP that showed excess Ca(II) ions increased the melting temperature by 10–20 °C,[25, 40, 51] Ca(II) did not appear to affect the thermal stability of MRP126 in this assay.

We next employed analytical SEC to evaluate the quaternary structure of MRP126 and variants. We found that apo MRP126 and variants eluted at 12.1 mL (75 mM HEPES, 100 mM NaCl, pH 7.0 + 0.2 mM TCEP), which corresponds to a molecular weight of 26 kDa and is consistent with a homodimer under these conditions (Figure S5 and Table S4). Adding 2 mM Ca(II) to the sample and running buffer had negligible effect on the elution volume, indicating that Ca(II)-bound MRP126 and variants are also homodimers (Figures S3, S4, and S5). Thus, MRP126 does not tetramerize in the presence of Ca(II) as observed for hCP and mCP.[25, 38, 39, 40, 51, 52] In this regard, MRP126 behaves more similarly to S100A12, which exists as homodimers in the absence and presence of excess Ca(II)).[36]

MRP126 selectively depletes Zn from bacterial growth medium using its His_3Asp sites. We next investigated the metal-sequestering ability of MRP126 using an unbiased metal-depletion assay previously reported by our lab.[28] We treated Tris:TSB medium with 8 μM of MRP126 or a variant at 30 °C for 20 h with shaking at 150 rpm and then spin-filtered each sample in a 10 kDa-molecular weight cut-off concentrator to remove MRP126 or variant and any bound metal ions. ICP-MS analysis of the medium revealed that treatment with MRP126 had negligible effect on the concentrations of Mn, Fe, Co, Ni, or Cu in Tris:TSB (Figure 2A-E), whereas the amount of Zn in the medium was reduced ≈20-30 fold (Figure 2F). Moreover, similar metal depletion occurred regardless of whether 2 mM Ca(II) and/or 3 mM BME was included in the medium. These conditions were evaluated because both Ca(II) and BME affect the metal-depletion profile of hCP.[28] These results indicate that MRP126 effectively depletes Zn, but not other first-

row transition metal ions, from Tris:TSB medium. The metal-depletion profile is similar to that of S100A12, which also provided Zn-selective depletion, and contrasts with the multi-metal depletion observed for CP (Figure 2). Thus, the metal-depletion profiles are consistent with those of characterized His_3Asp sites and differ from that of the His_6 site in CP.

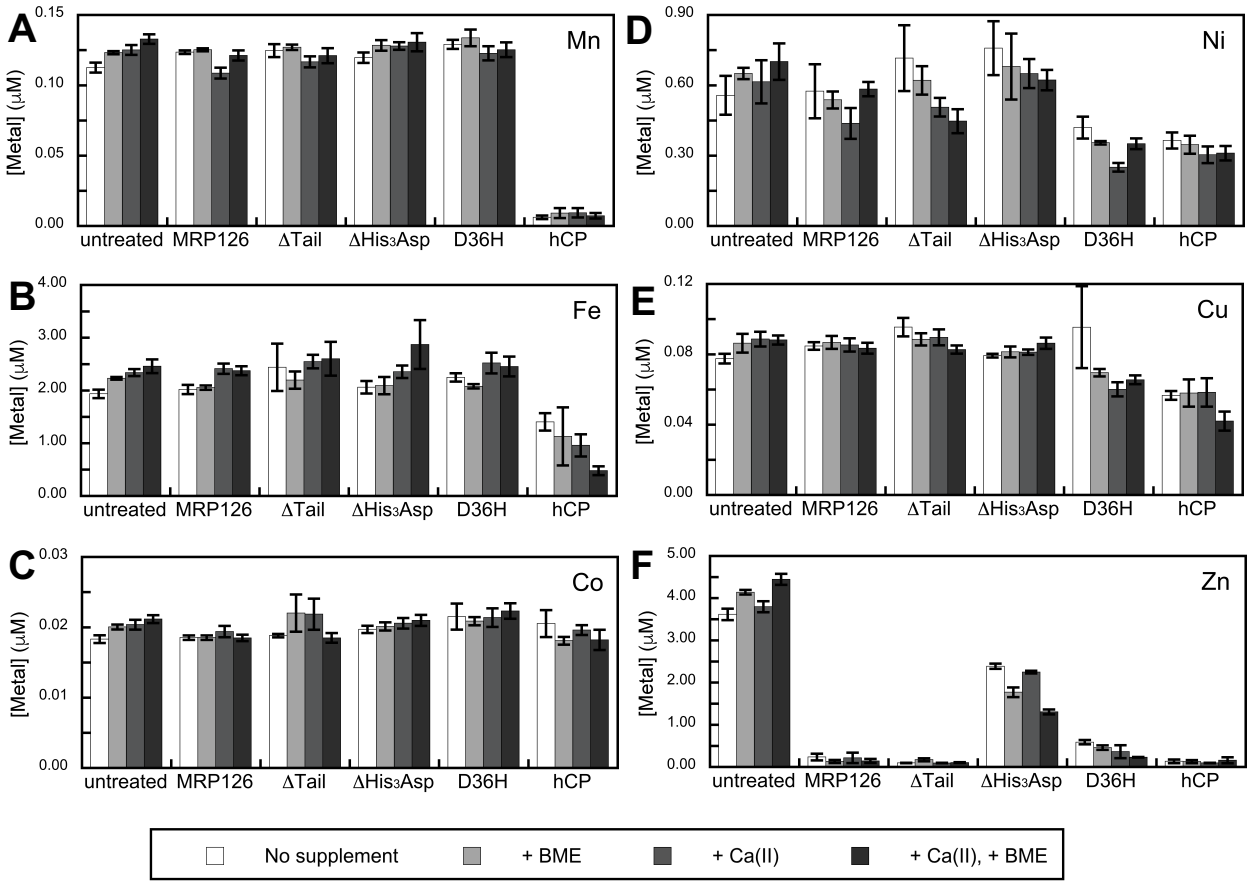

Figure 2. MRP126 selectively depletes Zn from bacterial growth medium using its His_3Asp sites. Depletion of (**A**) Mn, (**B**) Fe, (**C**) Co, (**D**) Ni, (**E**) Cu, and (**F**) Zn. Tris:TSB medium was incubated with 8 μM of MRP126, ΔTail, ΔHis_3Asp, D36H, or 10 μM hCP for 20 h at 30 °C. Following spin filtration to remove proteins > 10 kDa, the metal content of the filtrate was determined by ICP-MS (mean ± SEM, $n \geq 4$). The medium contained no supplement (white bars), a 3-mM BME supplement (light gray bars), a 2-mM Ca(II) supplement (medium gray bars), or both 2-mM Ca(II) and 3-mM BME supplements (dark gray bars). Raw ICP-MS data are provided in Table S5.

We also employed the metal-depletion assay to evaluate MRP126 variants and obtain insight into the site(s) contributing to Zn depletion. Treatment with the ΔHis_3Asp variant reduced the Zn content of the

medium by only ≈2 fold (Figure 2F), indicating that the conserved His_3Asp site is required for maximal Zn depletion by MRP126. In contrast, the ΔTail variant depleted Zn similarly to the native protein (Figure 2F), indicating that the histidine-rich tail is not essential for this process. Lastly, the D36H variant greatly reduced the Zn content of the medium, leaving slightly more Zn in the medium than seen with MRP126. The data also show that D36H, which likely has two His_4 sites at the homodimer interface, was more effective at sequestering Ni and perhaps Cu than native MRP126 (Figure 2D-E). Nevertheless, this mutation did not enhance Mn or Fe depletion (Figure 2A-B). Taken together, these data suggest that neither MRP126 nor the D36H variant create a 6-coordinate site using the His_3Asp/His_4 motif and two histidine residues from the tail region. Alternatively, if a 6-coordinate site forms, it exhibits a different metal-depletion profile from that of the His_6 site of CP.

In summary, these experiments demonstrated that MRP126 selectively sequesters Zn from Tris:TSB medium and that the conserved His_3Asp site, but not the histidine-rich tail, is required for full Zn depletion. These data suggest that the His_3Asp sites are high-affinity Zn(II) sites in MRP126. Moreover, the ΔHis_3Asp variant depleted some Zn from the medium, which indicates that additional sites in MRP126 provide relatively high-affinity Zn binding.

MRP126 restricts the growth of select microbes in a Ca(II)-dependent manner. Because the mammalian calgranulins exhibit antimicrobial activity that is attributed to metal sequestration, we next investigated the growth inhibitory activity of MRP126 and variants against a panel of microbes that were previously shown to be susceptible to S100A12 and/or hCP.[25, 27, 28, 36] These organisms include the Gram-negative bacteria *E. coli* and *Acinetobacter baumannii*, the Gram-positive bacteria *Staphylococcus aureus*, *Listeria monocytogenes*, and *Lactobacillus plantarum*, and the opportunistic fungal pathogen *Candida albicans*. In addition, we tested two serovars of the Gram-negative pathogen *Salmonella enterica*, one of which (*S.* Enteritidis) was previously shown to stimulate MRP126 expression during infection in chickens.[44, 46]

We performed standard antimicrobial activity assays with mid-log phase cultures in medium prepared with and without a 2-mM Ca(II) supplement using MRP126 as well as hCP and S1000A12 (Figure 3). MRP126 inhibited the growth of several microbes, most notably *L. monocytogenes* (Figure 3G), *L. plantarum* (Figure 3H), and *C. albicans* (Figure 3I). In contrast, MRP126 had a modest inhibitory effect on

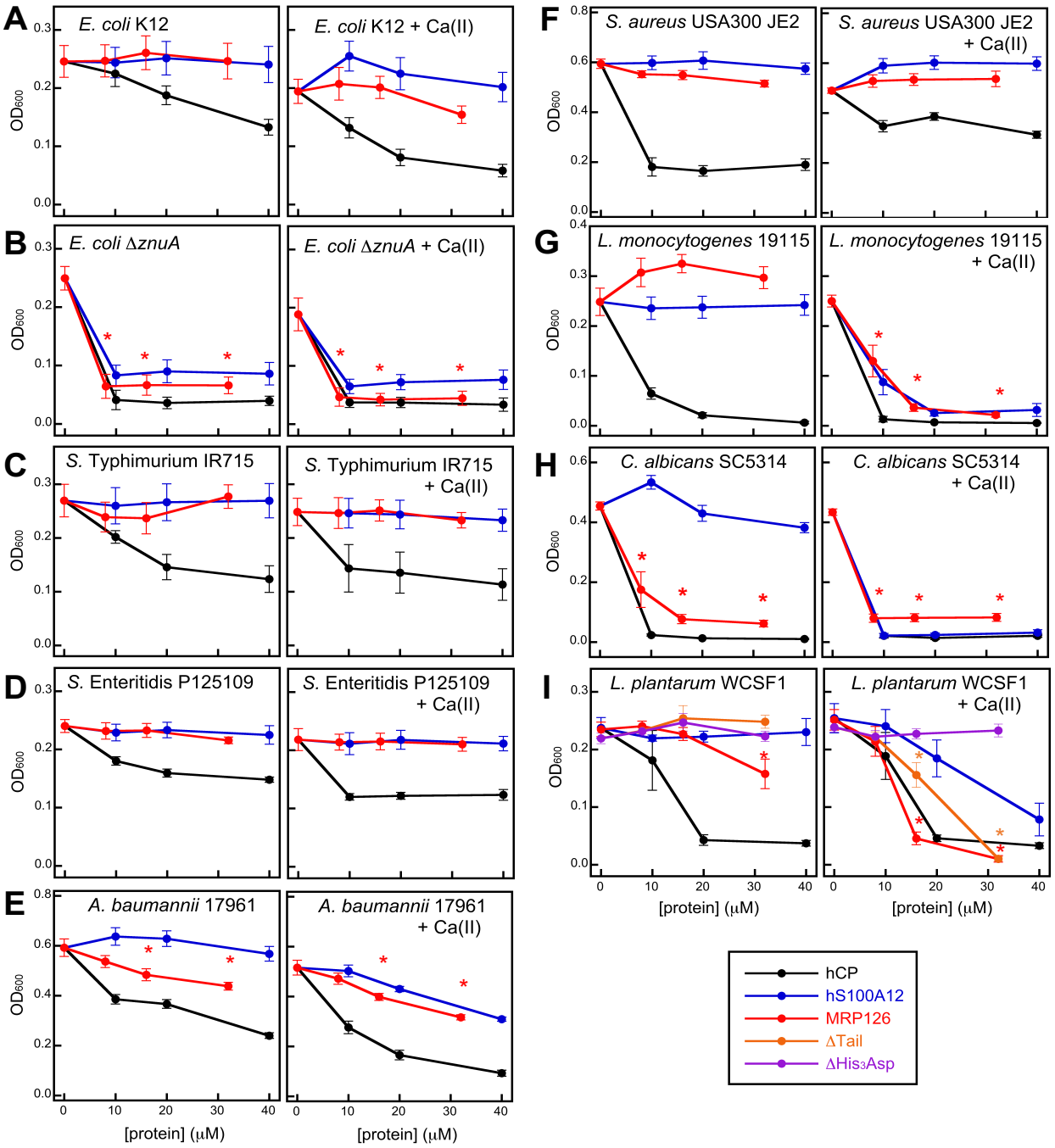

Figure 3. MRP126 inhibits the growth of select microbes in a Ca(II)-dependent manner. Growth inhibitory activity of hCP (black), S100A12 (blue), and MRP126 (red) against (**A**) *E. coli* K12, (**B**) *E. coli* Δ*znuA* (**C**), *S.* Typhimurium IR715,[54] (**D**) *S.* Enteritidis P125109,[55] (**E**) *A. baumannii* 17961, (**F**) *S. aureus* USA300 JE2, (**G**) *L. monocytogenes* 19115, (**H**) *C. albicans* SC5314, and (**I**) *L. plantarum* WCSF1. The ΔTail (orange), and ΔHis$_3$Asp (purple) MRP126 variants were also tested for activity against *L. plantarum*. Microbes were grown in the appropriate AMA medium ± 2 mM Ca(II) at 37 °C for 8 h for all bacteria or 20 h for *C. albicans* before the OD_{600} was measured (mean ± SEM, $n \geq 4$). Asterisks (*) indicate the concentrations of MRP126 where statistically significant differences in culture OD_{600} were observed compared to the no protein condition ($p < 0.05$ in a two-tailed unpaired t-test). See Table S6 for additional microbial strain and growth information.

A. baumannii growth (Figure 3E) and it failed to inhibit the growth of *E. coli* (Figure 3A), *S.* Typhimurium (Figure 3C), *S.* Enteritidis (Figure 3D), and *S. aureus* (Figure 3F). Nevertheless, MRP126 prevented the growth of *E. coli* Δ*znuA*, which lacks a functional high-affinity ZnuABC Zn(II)-uptake system (Figure 3B). This result indicates that the antimicrobial activity of MRP126 comes from Zn(II) deprivation. Overall, the antimicrobial activity profile of MRP126 is similar to that of S100A12, which selectively sequesters Zn from Tris:TSB and other media.[36, 53] In contrast, hCP restricted the growth of all evaluated organisms, at least to some degree, which we attribute to its broader metal-sequestration ability (Figure 2). We reason that the organisms exhibiting susceptibility to S100A12 and MRP126 are more sensitive to Zn(II) limitation than the organisms that only show susceptibility to hCP, at least under these experimental conditions.

These data also revealed a Ca(II) effect for some organisms. In particular, supplementation of the medium with Ca(II) was critical for MRP126 antimicrobial activity against *L. monocytogenes* and *L. plantarum* (Figures 3G and I). Thus, in terms of Ca(II) dependence, MRP126 is similar to S100A12, hCP, and mCP. [25, 27, 28, 36, 40]

Lastly, we compared the ability of the ΔTail and ΔHis_3Asp variants to suppress the growth of *L. plantarum* (Figure 3I). The ΔTail variant inhibited growth of this species, but not as effectively as native MRP126 at an intermediate concentration (16 μM). In contrast, the ΔHis_3Asp variant showed no growth inhibitory activity at any tested concentration. Thus, the canonical His_3Asp site of MRP126 is required for full antimicrobial activity against *L. plantarum* – and likely other organisms – under these conditions. Taken together with the metal-depletion studies and similarities to S100A12, these data further support the notion that the antimicrobial ability of MRP126 results from its ability to restrict Zn availability.

MRP126 homodimers bind multiple equivalents Zn(II) with Ca(II)-dependent affinity. Guided by the metal-depletion and antimicrobial activity assay results, we examined the effect of Zn(II) binding on the biophysical properties of MRP126. Providing an excess of Zn(II) (12.5 equivalents) did not change the CD spectrum of MRP126 in the absence or presence of 2 mM Ca(II) (Figure 4A), indicating that major changes to the predominantly α-helical secondary structure did not occur. Nevertheless, Zn(II) stabilized the folded protein in the thermal denaturation assay (Figure 4B), as heating to 95 °C failed to fully denature the Zn(II)-bound protein. In addition, pre-incubation of MRP126 with Zn(II) (4.4 equivalents) had negligible

impact on the analytical SEC elution volume (Figure 4C), indicating that the protein likely remains a homodimer after binding Zn(II).

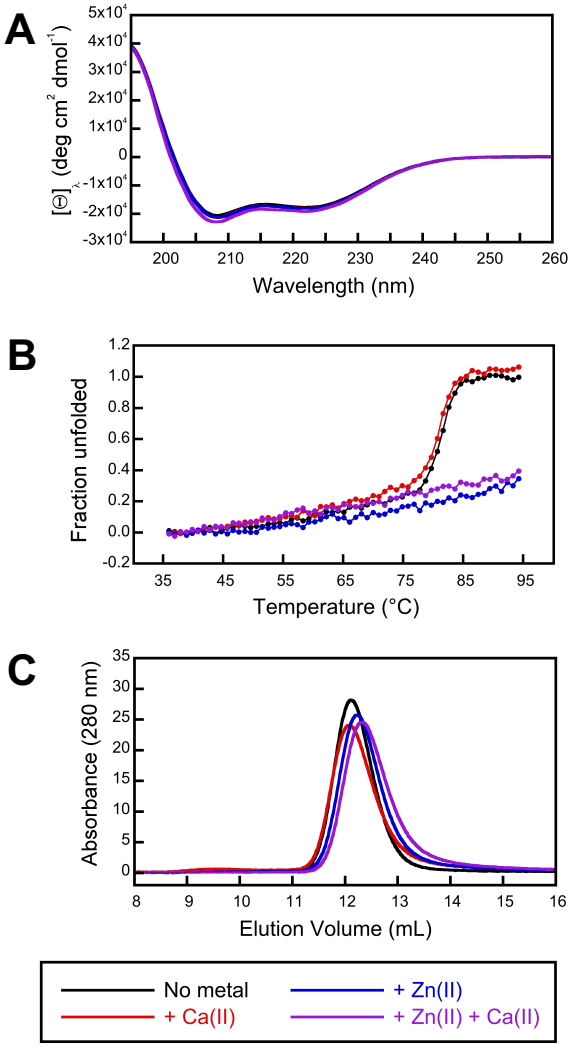

Figure 4. Zn(II) has negligible effect on the secondary structure and oligomerization state of MRP126 but does enhance its thermal stability. (**A**) CD spectra of MRP126 (8 μM) in 1 mM Tris-HCl, pH 7.5, with 0.2 mM TCEP at 25 °C and no metal added (black), 2 mM Ca(II) added (red), 100 μM Zn(II) added (blue), and 2 mM Ca(II) + 100 μM Zn(II) added (purple). Spectra are averages of three measurements and are representative of at least two independent experiments. (**B**) CD thermal denaturation of MRP126. Protein (as in panel A) was heated from 35 °C to 95 °C in 1 °C increments, and the CD magnitude was recorded at 226 nm. The relative change between the starting (T ≤ 40 °C) value and ending (T ≥ 90 °C) value normalized to the change observed for the no metal condition is plotted. Data are averages of three independent experiments. (**C**) Analytical SEC chromatograms of MRP126 (80 μM) in 75 mM HEPES, 100 mM NaCl, pH 7.0, with 0.2 mM TCEP at 4 °C and no metal added (black), 2 mM Ca(II) added to sample and running buffer (red), 350 μM Zn(II) added to sample (blue), and 2 mM Ca(II) added to sample and running buffer with 350 μM Zn(II) added to sample (purple). Elution volumes are listed in Table S4. Data are representative of at least two independent experiments.

Next, to obtain insight about the stoichiometry of Zn(II) binding and the apparent Zn(II) affinities, we performed a series of Zn(II) competition experiments using three small-molecule Zn(II) sensors with varying Zn(II) affinities. We found that MRP126 outcompeted Zincon ($K_{d,Zn(II)} \approx 10$ μM[56, 57]) for approximately six equivalents Zn(II) in both the absence and presence of 2 mM Ca(II) (Figure 5A-B). MRP126 outcompeted MF2 ($K_{d,Zn(II)} \approx 30$ nM[58, 59]) for approximately four equivalents Zn(II) in the absence of Ca(II) (Figure 5C). At higher Zn(II) equivalents, the titration curve indicated competition between MRP126 and MF2 for the metal ion (Figure 5C). MRP126 could not compete with the Ca(II)-insensitive Zn(II) sensor ZP4 ($K_{d,Zn(II)} = 650$ pM[60]) in the absence of Ca(II) (Figure 5D); however, when excess Ca(II) ions were present in the buffer, MRP126 outcompeted ZP4 for approximately two equivalents Zn(II) before competition was observed for approximately one more equivalent Zn(II) (Figure 5E).

In combination, these results suggest that MRP126 has three distinct pairs of Zn(II)-binding sites, and that Ca(II) binding has a marked effect on Zn(II) binding to the two highest-affinity pairs of sites. To probe the Zn(II) affinities for these different sites, we fit the competition titration data to binding equilibria models (see Supporting Information, Figures 5C, 5E, S6-S15 and Table 1).

From the MF2 competition data, we calculated that, in the absence of Ca(II), MRP126 binds four equivalents Zn(II) with low-nanomolar affinity ($K_{d,Zn(II)} \approx 1$ nM) and an additional two equivalents with approximately 100-fold lower affinity ($K_{d,Zn(II)} \approx 100$ nM). From the ZP4 competition data, we calculated that MRP126 binds two equivalents Zn(II) with picomolar affinity ($K_{d,Zn(II)} \approx 20$ pM) and an additional two equivalents Zn(II) with low-nanomolar affinity ($K_{d,Zn(II)} \approx 4$ nM). We note that there is some discrepancy between the calculated high-affinity values from the MF2 competition titrations ($K_{d,Zn(II)} \approx 1$ nM) and our observation that MRP126 could not effectively compete with ZP4 in the absence of excess Ca(II). As a result, these values should be taken as estimates rather than precise values for the apparent Zn(II) dissociation constants.

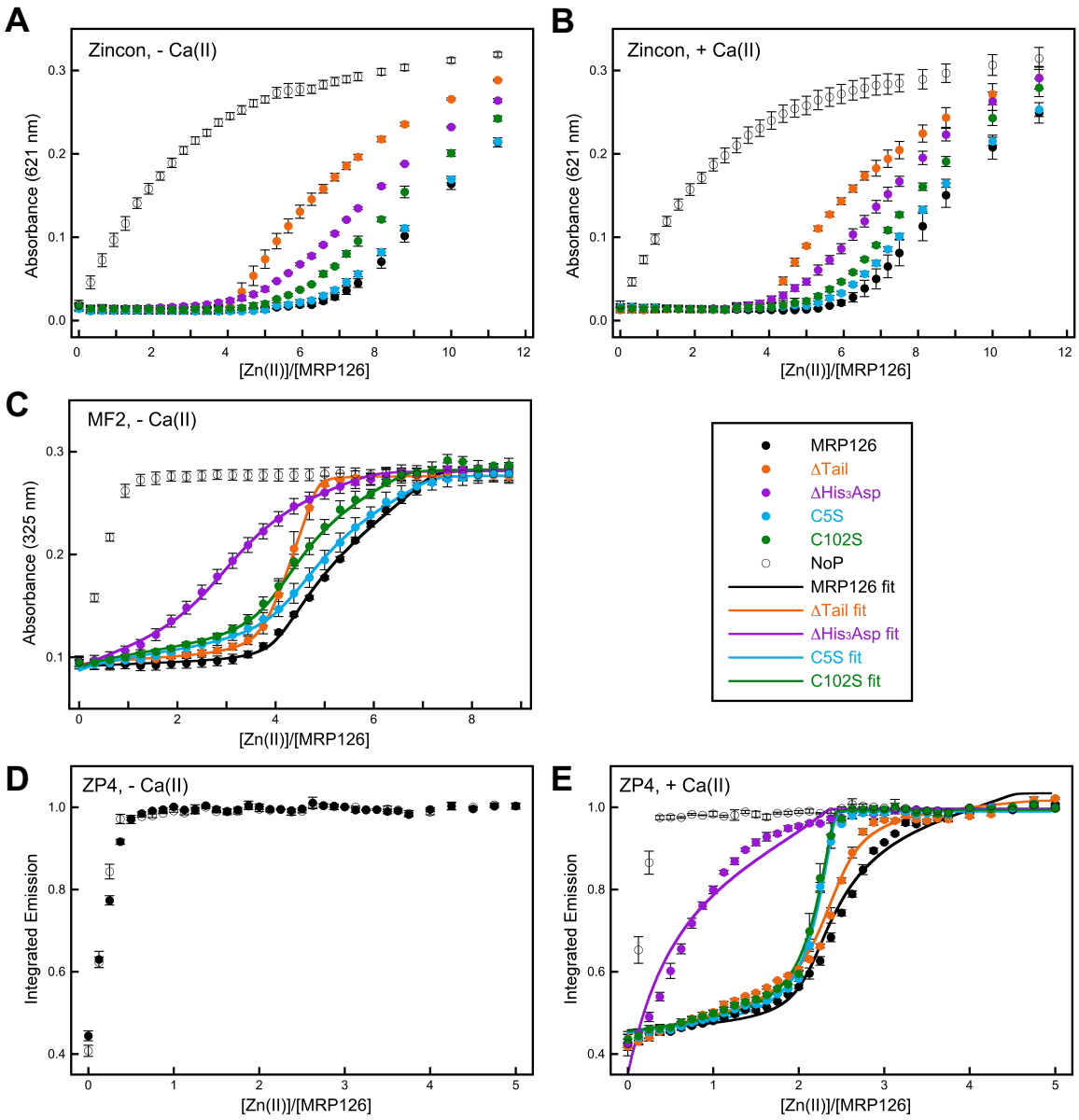

Figure 5. Zn(II)-competition titrations for MRP126 and variants inform the Zn(II)-binding sites and apparent affinities. All experiments were performed in 75 mM HEPES, 100 mM NaCl, pH 7.0, with 0.2 mM TCEP, with or without 2 mM Ca(II) as indicated. (**A-B**) Zincon ($K_{d,Zn(II)} \approx 10$ μM[56, 57]) competition experiments with 20 μM Zincon and 8 μM protein in the absence (**A**) or presence (**B**) of 2 mM Ca(II). Zn(II) was added 24x in 2.5 μM increments (0.31equivalents), 2x in 5 μM increments (0.63 equivalents), and 2x in 10 μM increments (1.25 equivalents). The absorbance at 621 nm was monitored to detect formation of the Zn(II)-Zincon complex. (**C**) MF2 ($K_{d,Zn(II)} \approx 30$ nM[58, 59]) competition experiments with 10 μM MF2 and 8 μM protein in the absence of Ca(II). Zn(II) was added 28x in 2.5 μM increments (0.31 equivalents). The absorbance at 325 nm was monitored to detect formation of the Zn(II)-MF2 complex. (**D-E**) ZP4 ($K_{d,Zn(II)}$ = 650 pM[60]) competition experiments with 1.5 μM ZP4 and 4 μM protein in the absence (**D**) or presence (**E**) of 2 mM Ca(II). Zn(II) was added 30x in 0.5 μM increments (0.13 equivalents) and 5x in 1 μM increments (0.25 equivalents). The increase in ZP4 fluorescence emission (λ_{ex} = 495 nm) indicated formation of the Zn(II)-ZP4 complex and was integrated from 505–650 nm. All data are averages ± SEM, *n* = 3. NoP = no protein

control titrations. Solid lines represent nonlinear regression fits to the data using Dynafit.[61] See Table 1 for a summary of these results, including calculated $K_{d,Zn(II)}$ values for MRP126 and variants. See also Figures S6-S10 and S11-S15 for simulated fits with higher and lower K_d values to these data.

MRP126 has three distinct pairs of Zn(II)-binding sites. Having established that MRP126 binds three pairs of Zn(II) ions, each with a distinct tier of affinities, we next aimed to identify which amino acid residues comprise each pair of binding sites. We therefore compared Zn(II) competition titrations of the ΔHis$_3$Asp, ΔTail, C5S, and C102S MRP126 variants to what we observed for the native protein (Figure 5 and Table 1). With Zincon both with and without Ca(II) (Figure 5A-B), ΔHis$_3$Asp shifted the titration curve by ≈2 equivalents from the WT, which indicates that each His$_3$Asp site coordinates one Zn(II) ion. ΔTail also shifted the titration curve such that a break occurred after ≈4 equivalents Zn(II). This result suggests that the C-terminal tail histidine residues contribute to at least one pair of Zn(II)-binding sites. In addition, C5S behaved similarly to the native protein, and C102S shifted the curve by ≈1 equivalent compared to native MRP126.

We obtained similar results from Zn(II) competition titrations with MF2 in the absence of Ca(II) (Figure 5C). ΔHis$_3$Asp outcompeted MF2 for ≈2 equivalents Zn(II) and thus shifted the titration curve by ≈2 equivalents from the native protein. ΔTail outcompeted MF2 for 4 equivalents Zn(II); however, compared to the native protein and the other variants, the rise in A_{325} after the break point was much steeper for ΔTail. This result indicates that the competition after four equivalents Zn(II) seen for native MRP126 arises from Zn(II) binding to sites that require the C-terminal histidine-rich tail. In addition, both the C5S and C102S variants had somewhat reduced competitiveness over the first four equivalents Zn(II) compared to the native protein, suggesting that both cysteine residues may contribute to the highest-affinity sites in the absence of Ca(II).

Table 1. MRP126 variant Zn(II)-binding stoichiometries and affinities from competition experiments.[a]

Zincon	**MRP126**	**ΔTail**	**ΔHis$_3$Asp**	**C5S**	**C102S**
– Ca(II), equiv Zn(II)	6.9	4.1	4.7	6.6	5.6
+ Ca(II), equiv Zn(II)	6.3	4.1	4.4	5.6	5.3

MF2, – Ca(II)	**MRP126**	**ΔTail**	**ΔHis$_3$Asp**	**C5S**	**C102S**
$K_{d,Zn(II)}$ Sites 1 + 2	1 ± 0.3 nM	1.6 ± 0.5 nM	7 ± 2 nM	5 ± 1 nM	4.3 ± 0.7 nM
equiv Zn(II)	4	4	2	4	4
$K_{d,Zn(II)}$ Site 3	80 ± 10 nM	--	190 ± 40 nM	130 ± 40 nM	150 ± 40 nM
equiv Zn(II)	2	0	2	2	2

ZP4, + Ca(II)	**MRP126**	**ΔTail**	**ΔHis$_3$Asp**	**C5S**	**C102S**
$K_{d,Zn(II)}$ Site 1	23 ± 4 pM	67 ± 8 pM	--	42 ± 4 pM	49 ± 5 pM
equiv Zn(II)	2	2	0	2	2
$K_{d,Zn(II)}$ Site 2	3.6 ± 0.4 nM	13 ± 2 nM	1.9 ± 0.2 nM	--	--
equiv Zn(II)	2	2	2	0	0

[a] Assays were performed as described in the legend for Figure 5. For Zincon, the equiv Zn(II) reported corresponds to the equivalents Zn(II) added to each MRP126 variant before A_{621} exceeded 0.032 (which corresponds to halfway between the A_{621} of the No Protein sample before and after the first Zn(II) addition). For MF2 and ZP4, the $K_{d,Zn(II)}$ values are reported from fitting the titration data to a model in which the indicated binding sites have the capacity for the equivalents Zn(II) listed below. Site 1 corresponds to the His_3Asp site, Site 2 corresponds to the Cys_2His_2 site, and Site 3 corresponds to the His_x site (see below).

With ZP4 in the presence of Ca(II), native MRP125, ΔTail, C5S, and C102S all clearly outcompeted the dye for two equivalents Zn(II), whereas ΔHis_3Asp did not (Figure 5E). Thus, the His_3Asp site indeed constitutes the highest-affinity Zn(II)-binding site in MRP126 in the presence of Ca(II). However, ΔHis_3Asp provided some competition over the course of the first two equivalents Zn(II), which demonstrates that other binding sites provide low-nanomolar Zn(II) affinity. Indeed, comparing the competition titrations after addition of 2 equivalents Zn(II) informs the composition of this middle-tier affinity site. Both C5S and C102S variants featured sharp increases in ZP4 fluorescence after the break point, suggesting that the residual

competition with the high-affinity dye seen with the native protein after this point depends on the presence of both native cysteine residues. The ΔTail competition titration curve featured an intermediate-steepness increase after two equivalents Zn(II), falling between the cysteine-to-serine variants and MRP126. This comparison suggests that one or more C-terminal tail histidine residues contribute to Zn(II) binding at the second-tier sites, but that it/they are not as critical as either C5 or C102.

Overall, from these titration curves and fitting the data to various models (see Supporting Information), we can conclude: (i) The conserved His_3Asp motifs constitute the two picomolar-affinity Zn(II)-binding sites (defined as Site 1 in our binding models) in the presence of Ca(II). (ii) Two non-conserved cysteines anchor a second pair of low-nanomolar Zn(II)-binding sites (Site 2) and the affinity of these sites also increases when excess Ca(II) ions are present. Also, these sites likely include at least one histidine residue from the C-terminal tail. (iii) The histidine-rich C-terminal tail provides a third-tier of Zn(II)-binding sites (Site 3) that coordinate the ion with high-nanomolar affinity and for which a Ca(II) effect was not observed.

Co(II)-binding titrations further inform the identities of the Zn(II)-binding sites. To further probe the coordination environments at the multiple Zn(II)-binding sites identified from the Zn(II) competition titrations, we titrated MRP126 and variants with Co(II) and monitored binding by optical absorption spectroscopy (Figures 6 and S16). For MRP126, the spectra (Figure 6A and F) were reminiscent of those previously reported for S100A12 and hCP as well as S100A7,[25, 36, 50] although with additional spectral features not seen for the human proteins as described below. For instance, in the presence of Ca(II) and ≈3 equivalents Co(II) (Figure 6F, bold trace), the solution of MRP126 was magenta and the optical absorption spectrum of this sample in the region corresponding to *d*–*d* transitions exhibits a broad signal centered at 563 nm with a shoulder at 525 nm, which is consistent with a 4- or 5-coordinate Co(II) species and closely resembles the Co(II) spectra assigned to the His_3Asp sites of hCP and S100A12.[25, 36] Thus, this result indicated that MRP126 indeed coordinates transition metal ions using its His_3Asp sites. It also rules out a six coordinate site comprised of the His_3Asp site and two additional ligands.

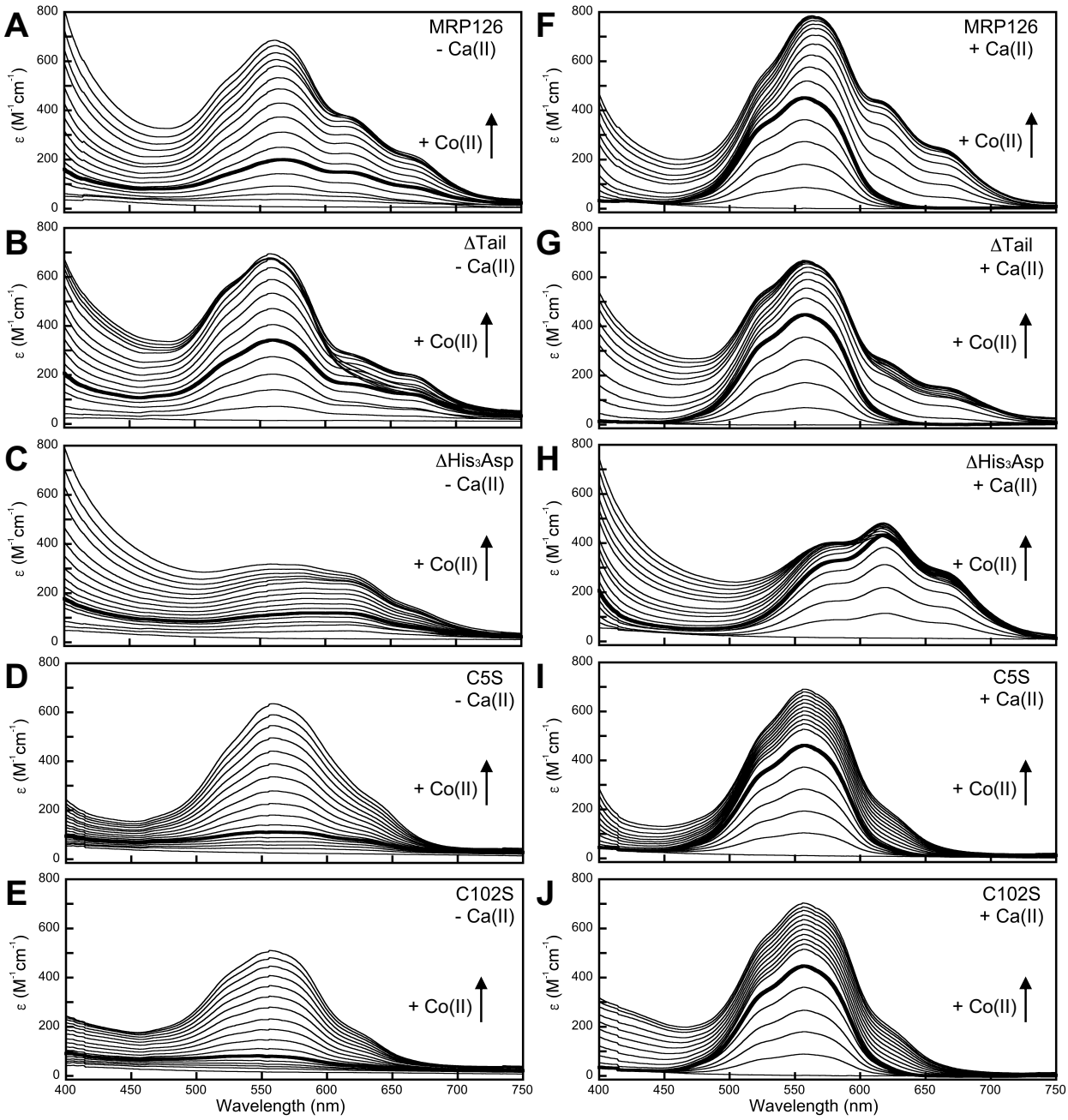

Figure 6. Co(II)-binding titrations indicate different metal-binding motifs for MRP126 variants. Optical absorption spectra for Co(II)-binding titrations (0-10 equivalents) of MRP126 and variants (240 μM) in 75 mM HEPES, 100 mM NaCl, pH 7.0, with 0.2 mM TCEP with (**A**-**E**) no Ca(II) added or (**F**-**J**) 6 mM Ca(II) added. (**A**,**F**) MRP126, (**B**,**G**) ΔTail, (**C**,**H**) ΔHis$_3$Asp, (**D**,**I**) C5S, (**E**,**J**) C102S. Each line represents an addition of 150 μM Co(II) (0.625 equivalents). In each panel, the spectrum corresponding to 3.1 equivalents Co(II) is shown as a bolder line. The ε values were calculated assuming that all metal-binding sites occur in pairs in the MRP126 homodimer; these values therefore encompass at least two distinct Co(II)-protein interactions for most variants. All panels are representative of at least two independent experiments. See also Figure S16 for versions of these plots that include the 300–400 nm range.

In the presence of Ca(II), the spectra of the ΔTail, C5S, and C102S variants (Figure 6G, I, and J) all looked nearly identical to that of MRP126 after ≈3 equivalents Co(II) were added, indicating that these variants also bind transition metal ions with the His_3Asp motif. In contrast, the spectra for ΔHis_3Asp (Figure 6H) exhibited a completely different shape than observed for MRP126 and other variants. In the presence of Ca(II), ΔHis_3Asp had a saturable overall absorption peak centered at around 625 nm and declining to the baseline by 700 nm. This peak shape is similar to what has been reported for Co(II)-substituted Cys_2His_2 Zn(II)-binding sites in zinc-finger proteins,[62-64] whereas similar shoulders/side-peaks (although of different relative magnitudes than ours) were also seen around 575 nm and 675 nm in another zinc-finger Cys_2His_2 site.[65] We spectroscopically detected this second-tier Co(II)-binding site for MRP126 after >3 equivalents Co(II) were added in the presence of Ca(II) (Figure 6F). Indeed, the spectra of MRP126 with 10 equivalents Co(II) in the presence of Ca(II) appears to be a near summation of the absorption spectra of MRP126 with three equivalents Co(II) and that of the ΔHis_3Asp variant with 10 equivalents Co(II). Moreover, the spectral features between 600 and 700 nm that we attribute to likely Cys_2His_2 sites in MRP126 and the ΔHis_3Asp variant were less pronounced for Co(II)-bound ΔTail (Figure 6G) and especially for the Co(II)-bound C5S and C102S variants (Figure 6I and J). These results are consistent with a Cys_2His_2 site; for each variant, we expect that one ligand is lost, changing the primary coordination sphere.

Additional spectral evidence of the Cys_2His_2 site was seen in the 300–400 nm range, where we detected a sulfur-to-cobalt charge-transfer transition in the spectra of all five variants (Figure S16). As expected, the intensity of this transition was reduced by approximately 50% for the C5S and C102S variants that each lack one of the native cysteine residues. From spectral comparisons, we could not identify any features that definitively correspond to Co(II) binding at the proposed third-tier affinity Zn(II) sites composed primarily of the C-terminal tail histidine residues, which may reflect either the poor affinity of Co(II) for that site and/or that the magnitude of the extinction coefficient for this Co(II) site is relatively low. The latter effect was previously seen with the ΔHis_3Asp variant of hCP that binds Co(II) exclusively at its His_6 site with an extinction coefficient of ≈40 $M^{-1}cm^{-1}$.[25]

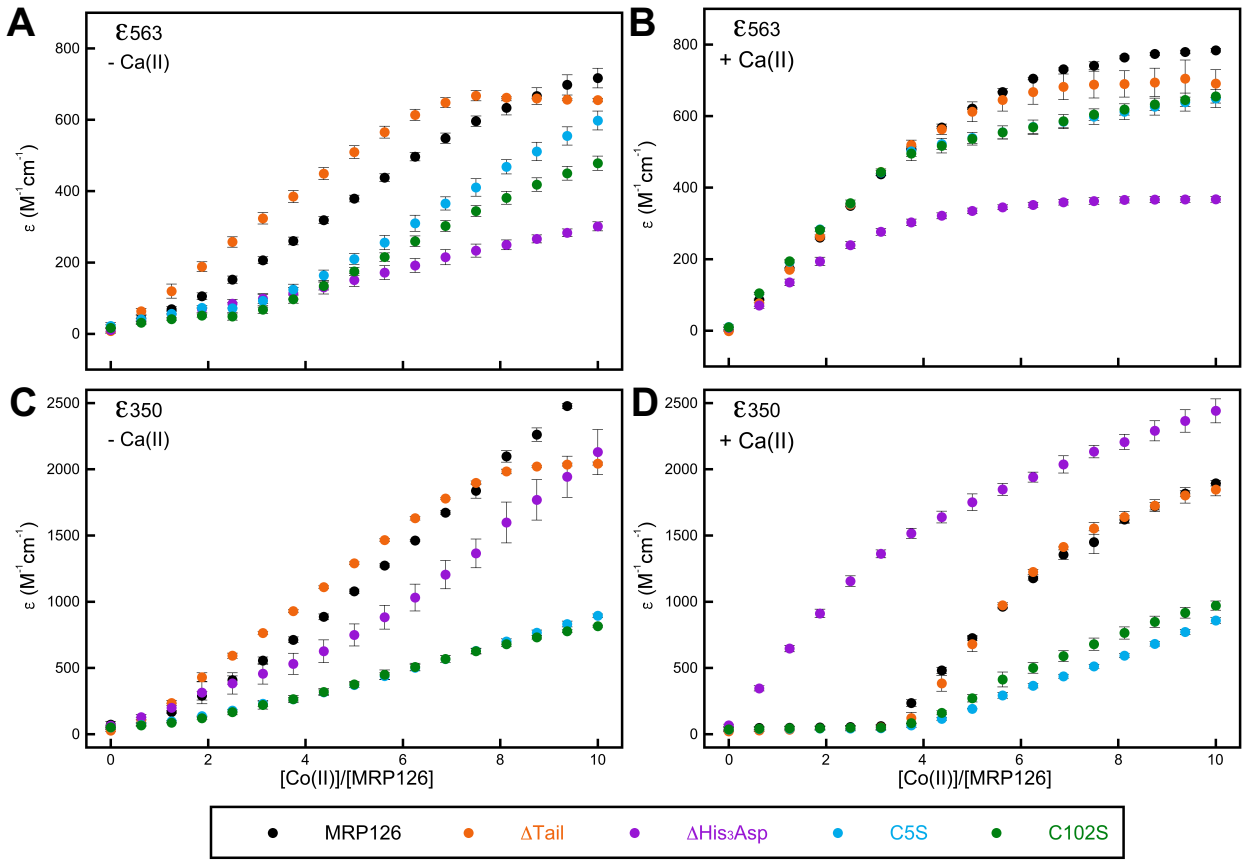

Figure 7. Optical absorption data indicate His_3Asp site fills first in presence of Ca(II). Optical absorption values for the Co(II) *d*–*d* transition at 563 nm corresponding to binding at the His_3Asp site (**A**-**B**) and a Co(II)–S charge transfer transition at 350 nm corresponding to binding to the Cys_2His_2 site (**C**-**D**), taken from the titrations seen in Figures 6 and S16 (mean ± SEM, n ≥ 2).

Ca(II) prioritizes metal-binding and delays metal-exchange at the His_3Asp sites. For all MRP126 variants, the Co(II) optical absorption spectral peaks did not show saturation behavior as quickly (if at all) in the absence of Ca(II) (Figure 6A-E), which likely reflects a lower affinity for Co(II) under these conditions that is consistent with our findings with Zn(II) (Figure 5D-E). To more easily compare the changes in the Co(II) spectra for each variant in the absence and presence of Ca(II), we plotted ε_{563} versus the Co(II) / MRP126 molar ratio to monitor the transition corresponding to Co(II) binding at the His_3Asp sites and ε_{350} versus the Co(II) / MRP126 molar ratio to monitor the transition that we attributed to sulfur-to-cobalt charge transfer at the Cys_2His_2 sites (Figure 7). In the presence of Ca(II) (Figure 7B and D), we detected an ordered

binding process for MRP126 as well as the ΔTail, C5S, and C102S variants. For the first ≈3 equivalents Co(II) added, ε_{563} increased linearly and negligible change in ε_{350} occurred, whereas at >3 equivalents Co(II) added, ε_{563} plateaued and ε_{350} increased dramatically. Thus, in the presence of excess Ca(II) ions, the His_3Asp sites preferentially filled with Co(II) and only after they were saturated was binding to the Cys_2His_2 sites detected. As expected, the ΔHis_3Asp variant immediately began to increase at ε_{350}, reflecting the Co(II) binding at the Cys_2His_2 sites. In contrast, in the absence of Ca(II) (Figure 7A and C), we did not observe any clearly ordered binding for the native protein, as both ε_{563} and ε_{350} simultaneously increased at the start of the Co(II) titration. Thus, Ca(II) appears to be essential for directing transition metal ions preferentially to the His_3Asp sites, as the His_3Asp and Cys_2His_2 sites appear to fill indiscriminately with Co(II) in the absence of Ca(II). These titrations also show that the binding of Ca(II) increases the transition-metal affinity of the His_3Asp sites, both in absolute terms and relative to the affinity of the Cys_2His_2 site. This behavior is reminiscent of prior studies of hCP, which showed that the presence of excess Ca(II) ions directs transition metals (e.g. Mn(II), Fe(II)) to the His_6 site.[33, 37]

Lastly, we investigated metal substitution by adding 10 equivalents Zn(II) to the Co(II)-bound proteins (Figure 8). In the presence of Ca(II), Zn(II) addition to the native protein resulted in disappearance of the spectral features for the Co(II)-bound protein between 600–700 nm that we attribute to the Cys_2His_2 site within 2 min, whereas the peak centered on 563 nm corresponding to the His_3Asp site decayed over the course of approximately 1 h (Figure 8A). Similar behavior was observed for the ΔTail, C5S, and C102S variants (Figure 8C, D, and E), with a noticeable acceleration in metal substitution for ΔTail. In contrast, for ΔHis_3Asp (Figure 8B), all signals for *d*–*d* transitions were lost within 2 min following Zn(II) addition. For the ΔTail variant in the absence of Ca(II), Zn(II) addition also eliminated all *d*–*d* transitions in a 2-min timeframe (Figure 8F) For the other Co(II)-bound variants in the absence of Ca(II), Zn(II) addition caused the protein to precipitate, precluding any time course measurements of metal substitution. Taken together, these results indicate that the Cys_2His_2 site has relatively fast metal substitution in either the absence or presence of Ca(II), whereas the His_3Asp site displays relatively slow metal exchange in the presence of Ca(II), but not in its absence. Overall, these observations are in accord with the results from the metal depletion and Zn(II) competition experiments and further indicate that Ca(II) binding helps prevent the loss of captured transition metal ions at the His_3Asp sites of MRP126.

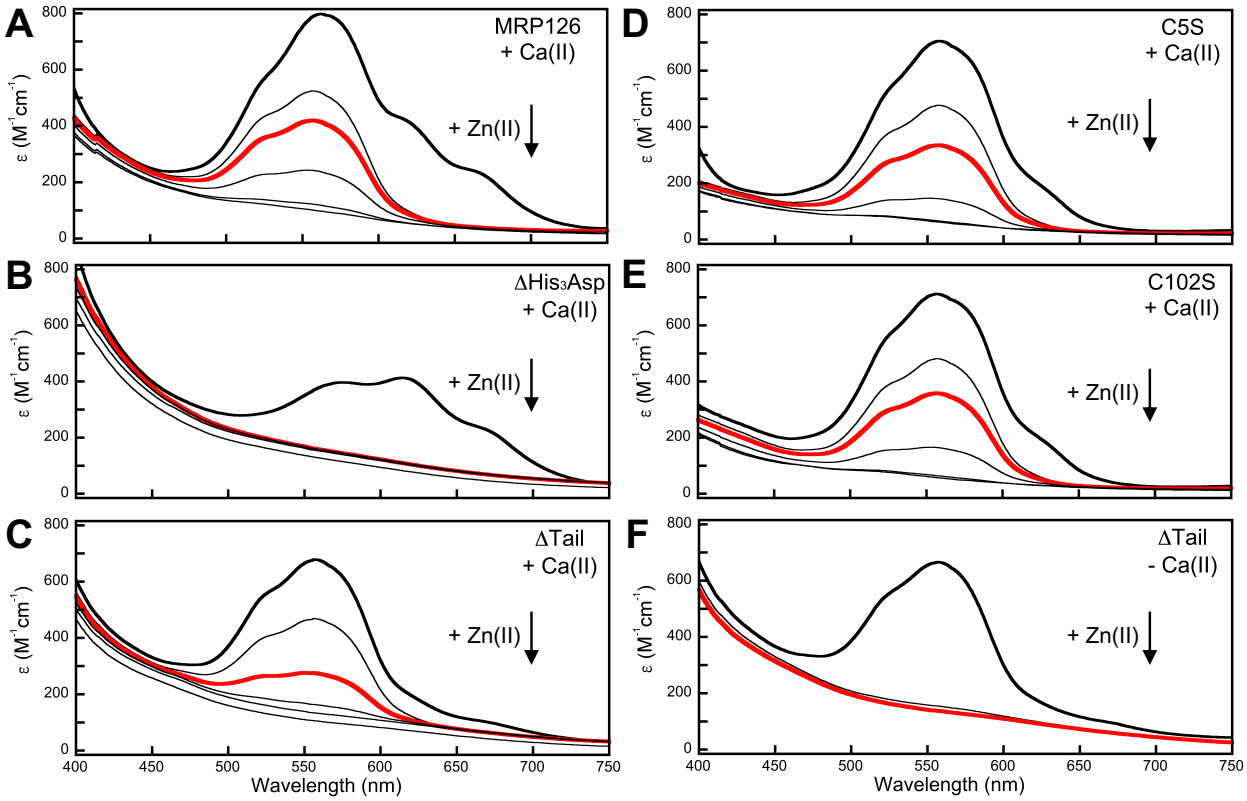

Figure 8. His_3Asp sites kinetically trap transition metals in the presence of Ca(II). Optical absorption spectral time course of Zn(II) (10 equivalents) replacement of Co(II) (10 equivalents) in 75 mM HEPES, 100 mM NaCl, pH 7.0, with 0.2 mM TCEP with 6 mM Ca(II) added (**A**-**E**) or no Ca(II) added (**F**). The lines represent spectra before Zn(II) addition (bold line) and after 2 min, 6 min (bold red line), 20 min, 60 min, and 120 min. (**A**) MRP126, (**B**) Δ His_3Asp , (**C**) ΔTail , (**D**) C5S, (**E**) C102S, (**F**) ΔTail without Ca(II). Only 2 and 6 min time points were collected for ΔTail without Ca(II). Adding Zn(II) to the other Co(II)-bound MRP126 variants in the absence of Ca(II) caused immediate protein precipitation, which precluded similar time course measurements. ε values were calculated assuming two binding sites per dimer. All panels are representative of at least two independent experiments.

Discussion

In this work, we evaluated the biophysical, metal-binding, and antimicrobial properties of an avian calgranulin homolog of mammalian CP and S100A12 to provide insights into the ancestral function of this protein family and better understand the subsequent divergence in function among extant homologs (as summarized in Figure S17). We selected chicken MRP126 because of previous studies implicating it in the innate immune response to bacterial infection[43-47] and identifying a conserved role in inflammatory

signaling.[6] Our studies reveal several key similarities and differences between MRP126 and its mammalian homologs. Unlike CP, which forms tetramers, [25, 38, 39, 40, 52, 66, 67] and S100A12, which forms higher-order oligomers (possibly tetramers or hexamers),[35, 41, 42] MRP126 exists exclusively as a dimer under the conditions employed in this study (Figure 4). This result suggests that the ancestral homolog was likely dimeric, with the higher-order oligomerization properties of mammalian homologs evolving more recently. The Zn-selective metal-depletion profile displayed by MRP126 (Figure 2) mirrors the behavior of S100A12,[36] rather than the broader metal-depletion profile (including Mn, Fe, and Ni) seen with CP[28, 40] Parsimony therefore suggests that Zn(II) sequestration was the ancestral function of the calgranulin clade, and mammalian CP evolved its more promiscuous metal-sequestration ability after the homologs had diverged (and perhaps required the subsequent divergence and complementary evolution of S100A8 and S100A9). D36H, an MRP126 variant engineered to have a His_4 site similar to the His_4 site of CP, showed improved Ni depletion compared to the native protein (Figure 2D), providing some insight into how evolution may have begun to expand the selectivity profile of the ancestral protein. However, unlike CP, the D36H variant depleted neither Mn nor Fe. Previous work with variants of CP lacking either or both histidine residues in the S100A9 C-terminal tail that complete the His_6 site coordination sphere showed importance of those residues for Mn(II) and Fe(II) capture.[26, 28, 32, 68] These results therefore suggest that the D36H variant of MRP126 does not form a CP-like His_6 site. Thus, further protein evolution that enabled the histidine-rich C-terminal tail to participate in a transition-metal-binding site at the dimer interface was likely necessary to impart this advantageous property to CP.

The apparent Zn(II) selectivity of MRP126 likely results in its diminished antimicrobial activity profile compared to hCP (Figure 3). Along these lines, in the antimicrobial activity assays, MRP126 performed similarly to S100A12, which sequesters Zn(II) but not other metal nutrients like Mn(II) and Fe(II).[36] Bird and reptile species each express this lone calgranulin homolog, and it remains an open question whether these organisms have evolved any compensatory mechanism – perhaps involving unrelated proteins or more-distantly-related S100s – to provide the missing Mn(II)/Fe(II) sequestration ability imparted by CP. If those species indeed lack such compensatory proteins, our antimicrobial activity experiments with MRP126 (Figure 3) would suggest that the bird/reptile innate-immune system has a less-potent arsenal than do mammals for implementing a nutritional-immunity defense against potential invaders.

As was previously seen for CP and S100A12,[25, 36, 40] the presence of excess Ca(II) ions at a concentration that mimics the extracellular environment enhanced the antimicrobial activity of MRP126, most notably against *L. monocytogenes* and *L. plantarum* (Figure 3G and I). This finding agreed with the Ca(II)-dependent increase in Zn(II)-binding affinity of MRP126 as measured by competition with ZP4 (Figure 5D and E). It is also reminiscent of prior observations of Ca(II) enhancing the Zn(II) affinities of the His_3Asp and His_6 sites of hCP.[25] Therefore, the ability of Ca(II) to enhance transition-metal binding affinity appears to be an ancestral property of the calgranulin family, although other effects of Ca(II) binding (such as changes to quaternary structure) have clearly diverged. S100A7 (psoriasin), a more distantly-related S100 protein, also has two His_3Asp sites, sequesters Zn(II) and performs an apparent innate-immune role.[50, 69, 70] Whereas Ca(II) binding affected the midpoint potential of two intramolecular disulfide bonds in the S100A7 homodimer, Ca(II) did not as clearly enhance the Zn(II) affinity or antimicrobial potency of this protein.[50] This comparison suggests that the ancestral calgranulin evolved the ability to use Ca(II) to modulate its transition-metal-binding sites, thereby leveraging higher extracellular Ca(II) concentrations to convert to a higher-affinity state upon release from the cytoplasm at infection sites.

In contrast to hCP and S100A12, which each have two high-affinity Zn(II) sites per dimer,[25, 27, 36] MRP126 binds additional equivalents Zn(II) (Figure 5). Based on the Zn(II) competition titrations (Figure 5) and Co(II)-binding studies (Figure 6), we present a model for Zn(II) binding to this protein (Figure 9). In the absence of Ca(II), Zn(II) binds with similar low-nanomolar affinity to the two conserved His_3Asp sites at the homodimer interface as well as the two Cys_2His_2 sites comprised of Cys5 from one monomer, Cys102 from the second monomer, and (likely) His98 (based on its location on the same face of the helix one turn below C102) and a C-terminal tail His from the second monomer. Additional Zn(II) ions can then bind with high-nanomolar affinity to two sites primarily or entirely comprised of C-terminal tail histidine residues (His_x sites) from each monomer. In the presence of excess Ca(II), the Zn(II) affinities of the His_3Asp and Cys_2His_2 sites are enhanced. The first two Zn(II) equivalents bind to the His_3Asp sites with low-picomolar affinity, the next two Zn(II) equivalents bind to the Cys_2His_2 sites with improved but still low-nanomolar affinity, and two additional Zn(II) equivalents then bind with high-nanomolar affinity to the His_x sites. This ability of Ca(II) to prioritize one type of transition-metal-binding site over another echoes previous findings with hCP where

providing Ca(II) imparts a preference for Fe(II) to bind to the His_6 site over the His_3Asp site[37] and Mn(II) to bind to the His_6 site over either the His_3Asp site or the EF-hand sites.[33]

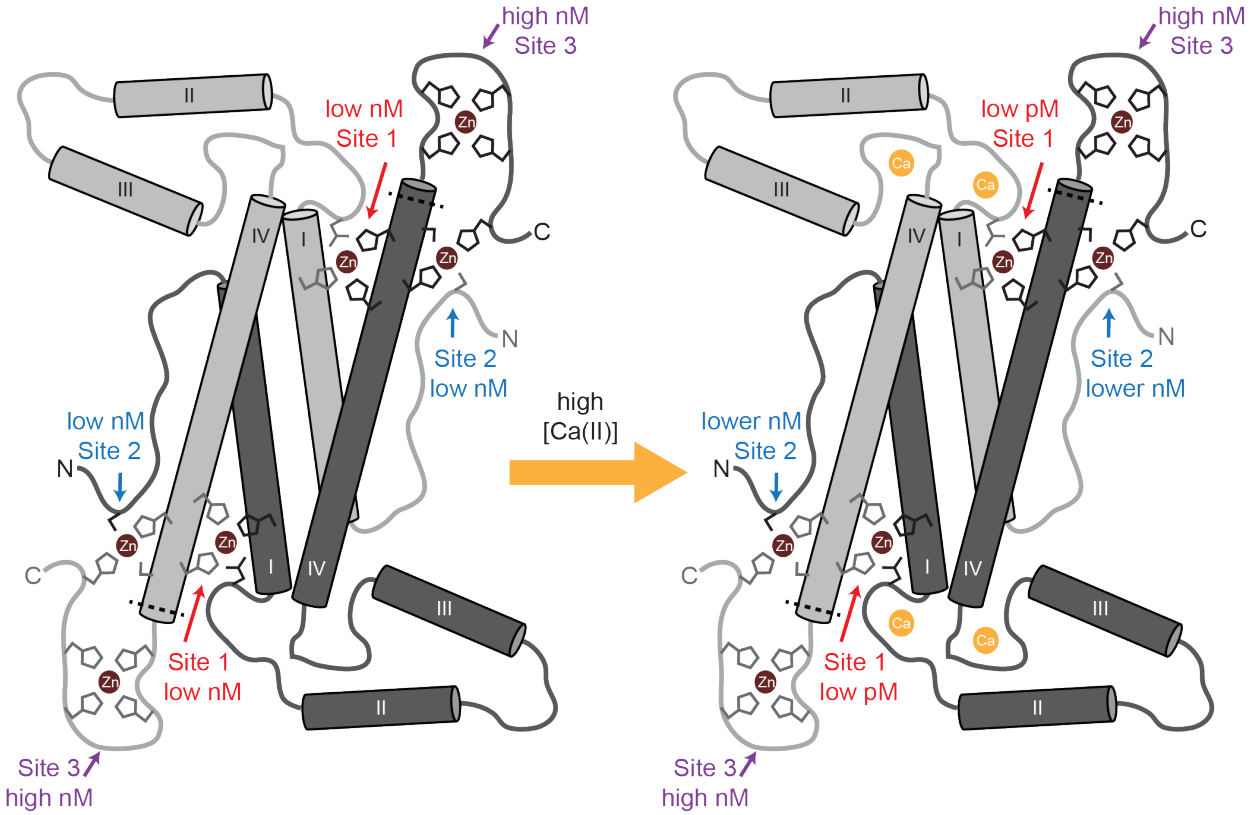

Figure 9. Model of MRP126 Ca(II)-dependent Zn(II) binding. Each MRP126 homodimer contains three distinct pairs of Zn(II)-binding sites. Site 1 is a canonical calgranulin His_3Asp site comprised of His26 and Asp36 from one monomer and His96 and His100 from the other monomer. Site 2 is a dicysteine site that likely consists of Cys5 from one monomer and Cys102, His98, and a C-terminal tail histidine from the other monomer, which we denote Cys_2His_2. Site 3 likely consists of multiple histidines from the C-terminal tail of one monomer, which we call His_x. In the absence of Ca(II), Zn(II) binds to MRP126 with similar low-nanomolar affinity at either Site 1 (His_3Asp) or Site 2 (Cys_2His_2), then with high-nM affinity at Site 3 (His_x). Ca(II) dramatically increases the affinity of Site 1 and increases the affinity of Site 2 to a lesser degree. Thus in the presence of Ca(II), Zn(II) preferentially binds with low-pM affinity to Site 1 (His_3Asp), then with lower-nanomolar affinity to site Site 2 (Cys_2His_2), and finally with high-nanomolar at Site 3 (His_x). The primary coordination sphere for the His_x site is unknown and it is drawn as a His_4 site. The dashed line indicates the approximate location of the point of truncation for the ΔTail variant.

The importance of these additional Zn(II)-binding sites to the Zn(II)-sequestering, antimicrobial role of MRP126 is unclear. Neither of the cysteine residues that participate in Zn(II) binding is conserved within bird and reptile MRP126 homologs (Figure S1); however, these cysteine residues always appear as a pair in the homologs that do have them. It is also possible that, in an oxidizing environment, these cysteine

residues could form a disulfide bond and thereby eliminate the Cys_2His_2 Zn(II)-binding site and perhaps alter the Zn(II) affinity of the His_3Asp site. In contrast, a histidine- (and glutamine-) rich C-terminal tail does appear to be a hallmark feature of this clade of the calgranulin family (Figure S1), which may suggest that the moderate-affinity Zn(II) binding it affords confers a functional advantage to the protein. The ΔHis_3Asp variant depleted some Zn from bacterial growth medium (Figure 2F) but did not affect the growth of *L. plantarum* (Figure 3I), whereas the ΔTail variant depleted Zn similarly to the native protein (Figure 2F) and had a slightly attenuated antimicrobial effect on *L. plantarum* (Figure 3I). From these results, it appears that the intact His_3Asp sites are necessary and sufficient for MRP126 to function as a Zn(II)-sequestering protein, but future studies with additional variants could help determine whether the presence of the additional Zn(II)-binding sites offers functional advantages.

Conclusions

In conclusion, we demonstrated that an avian calgranulin homolog, chicken MRP126, sequesters Zn(II) in a Ca(II)-dependent manner to restrict the growth of certain microbes. MRP126 shares these functional properties with mammalian S100A12 and the His_3Asp site of CP, which indicates that an ancestral calgranulin had already evolved similar traits in the last common ancestor of higher vertebrates.

Accession Codes

Chicken (*Gallus gallus*) MRP126, Uniprot: P28318

Human (*Homo sapiens)* S100A8, Uniprot: P05109

Human (*Homo sapiens*) S100A9, Uniprot: P06702

Human (*Homo sapiens*) S100A12, Uniprot: P80511

Acknowledgements

We gratefully acknowledge the NIH (R01GM118695) for financial support. We thank Dr. Richard Schiavoni at the Koch Institute for performing the trypsin digest and LC-MS/MS identification of the higher molecular weight gel band of MRP126. The ICP-MS instrument is housed in the MIT Center for Environmental Health Sciences Bioanalytical Core supported by NIH grant P30-ES002109. The MIT Biophysical Instrumentation

Facility for the Study of Complex Macromolecular Systems is supported by NSF grant 0070319. The QToF mass spectrometer is housed in the MIT Department of Chemistry Instrumentation Facility. The *S. aureus* USA300 JE2 strain was obtained from the Network on Antimicrobial Resistance in *Staphylococcus aureus* (NARSA) program supported under NIAID/NIH contract no. HHSN272200700055C.

Abbreviations

AMA	antimicrobial activity
ATCC	American Type Culture Collection
BHI	brain heart infusion medium
BME	β-mercaptoethanol
CD	circular dichroism
CP	calprotectin
hCP	human calprotectin (including hCP-Ser, the Cys → Ser variant)
mCP	murine calprotectin (including mCP-Ser, the Cys → Ser variant)
DTT	dithiothreitol
HEPES	4-(2-hydroxyethyl)-1-piperazineethanesulfonic acid
ICP-MS	inductive-coupled plasma mass spectrometry
IPTG	isopropyl β-d-1-thiogalactopyranoside
LB	Luria–Bertani medium
LC-MS	liquid chromatography mass spectrometry
MF2	Mag-fura-2
MRS	De Man, Rogosa, and Sharpe medium
PDB	Protein Data Bank
PMSF	phenylmethylsulfonylfluoroide
SEC	size exclusion chromatography
SEM	standard error of the mean
TCEP	tris(2-carboxyethyl)phosphine
Tris	tris(hydroxymethyl)aminomethane

TSB	tryptic soy broth medium
YPD	yeast extract peptone dextrose medium
ZP4	Zinpyr-4
ΔHis$_3$Asp	H26N/D36S/H96N/H100N quadruple mutant variant of MRP126
ΔTail	H105Stop variant of MRP126

Supporting Information

Complete experimental methods, Tables S1-S6, and Figures S1-S17, and supporting references. This material is available free of charge via the Internet at http://pubs.acs.org.

References

[1] Marenholz, I., Heizmann, C. W., and Fritz, G. (2004) S100 proteins in mouse and man: from evolution to function and pathology (including an update of the nomenclature), *Biochem. Biophys. Res. Commun. 322*, 1111-1122.

[2] Donato, R., Cannon, B. R., Sorci, G., Riuzzi, F., Hsu, K., Weber, D. J., and Geczy, C. L. (2013) Functions of S100 proteins, *Curr. Mol. Med. 13*, 24-57.

[3] Zimmer, D. B., Eubanks, J. O., Ramakrishnan, D., and Criscitiello, M. F. (2013) Evolution of the S100 family of calcium sensor proteins, *Cell Calcium 53*, 170-179.

[4] Wheeler, L. C., Donor, M. T., Prell, J. S., and Harms, M. J. (2016) Multiple evolutionary origins of ubiquitous Cu^{2+} and Zn^{2+} binding in the S100 protein family, *PlosOne 11*, e0164740.

[5] Zygiel, E. M., and Nolan, E. M. (2018) Transition metal sequestration by the host-defense protein calprotectin, *Annu. Rev. Biochem. 87*, 621-643.

[6] Loes, A. N., Bridgham, J. T., and Harms, M. J. (2018) Coevolution of the Toll-like receptor 4 complex with calgranulins and lipopolysaccharide, *Front. Immunol. 9*, 304.

[7] Edgeworth, J., Gorman, M., Bennett, R., Freemont, P., and Hogg, N. (1991) Identification of P8,14 as a highly abundant heterodimeric calcium-binding protein complex of myeloid cells, *J. Biol. Chem. 266*, 7706-7713.

[8] Guignard, F., Mauel, J., and Markert, M. (1995) Identification and characterization of a novel human neutrophil protein related to the S100 family, *Biochem. J. 309 (Pt 2)*, 395-401.

[9] Pietzsch, J., and Hoppmann, S. (2009) Human S100A12: a novel key player in inflammation?, *Amino Acids 36*, 381-389.

[10] Wang, S. W., Song, R., Wang, Z. Y., Jing, Z. C., Wang, S. X., and Ma, J. (2018) S100A8/A9 in inflammation, *Front. Immunol. 9*, 1298.

[11] Ryckman, C., Vandal, K., Rouleau, P., Talbot, M., and Tessier, P. A. (2003) Proinflammatory activities of S100: Proteins S100A8, S100A9, and S100A8/A9 induce neutrophil chemotaxis and adhesion, *J. Immunol. 170*, 3233-3242.

[12] Ehrchen, J. M., Sunderkötter, C., Foell, D., Vogl, T., and Roth, J. (2009) The endogenous Toll-like receptor 4 agonist S100A8/S100A9 (calprotectin) as innate amplifier of infection, autoimmunity, and cancer, *J. Leukoc, Biol. 86*, 557-566.

[13] Foell, D., Wittkowski, H., Kessel, C., Lüken, A., Weinhage, T., Varga, G., Vogl, T., Wirth, T., Viemann, D., Björk, P., van Zoelen, M. A. D., Gohar, F., Srikrishna, G., Kraft, M., and Roth, J. (2013) Proinflammatory S100A12 can activate human monocytes via Toll-like receptor 4, *Am. J. Respir. Crit. Care Med. 187*, 1324-1334.

[14] Vogl, T., Tenbrock, K., Ludwig, S., Leukert, N., Ehrhardt, C., van Zoelen, M. A. D., Nacken, W., Foell, D., van der Poll, T., Sorg, C., and Roth, J. (2007) Mrp8 and Mrp14 are endogenous activators of Toll-like receptor 4, promoting lethal, endotoxin-induced shock, *Nat. Med. 13*, 1042-1049.

[15] Riva, M., Källberg, E., Björk, P., Hancz, D., Vogl, T., Roth, J., Ivars, F., and Leanderson, T. (2012) Induction of nuclear factor-kappa B responses by the S100A9 protein is Toll-like receptor-4-dependent, *Immunology 137*, 172-182.

[16] Hofmann, M. A., Drury, S., Fu, C. F., Qu, W., Taguchi, A., Lu, Y., Avila, C., Kambham, N., Bierhaus, A., Nawroth, P., Neurath, M. F., Slattery, T., Beach, D., McClary, J., Nagashima, M., Morser, J., Stern, D., and Schmidt, A. M. (1999) RAGE mediates a novel proinflammatory axis: A central cell surface receptor for S100/calgranulin polypeptides, *Cell 97*, 889-901.

[17] Leclerc, E., Fritz, G., Vetter, S. W., and Heizmann, C. W. (2009) Binding of S100 proteins to RAGE: An update, *Biochim. Biophys. Acta, Mol. Cell Res. 1793*, 993-1007.

[18] Ma, L., Sun, P., Zhang, J.-C., Zhang, Q., and Yao, S.-L. (2017) Proinflammatory effects of S100A8/A9 via TLR4 and RAGE signaling pathways in BV-2 microglial cells, *Int. J. Mol. Med. 40*, 31-38.

[19] Hood, M. I., and Skaar, E. P. (2012) Nutritional immunity: transition metals at the pathogen-host interface, *Nat. Rev. Microbiol. 10*, 525-537.

[20] Kehl-Fie, T. E., and Skaar, E. P. (2010) Nutritional immunity beyond iron: a role for manganese and zinc, *Curr. Opin. Chem. Biol. 14*, 218-224.

[21] Skaar, E. P. (2010) The battle for iron between bacterial pathogens and their vertebrate hosts, *Plos Pathog. 6*, e1000949.

[22] Zackular, J. P., Chazin, W. J., and Skaar, E. P. (2015) Nutritional immunity: S100 proteins at the host-pathogen interface, *J. Biol. Chem. 290*, 18991-18998.
[23] Cunden, L. S., and Nolan, E. M. (2018) Bioinorganic explorations of Zn(II) sequestration by human S100 host-defense proteins, *Biochemistry 57*, 1673-1680.
[24] Kehl-Fie, T. E., Chitayat, S., Hood, M. I., Damo, S., Restrepo, N., Garcia, C., Munro, K. A., Chazin, W. J., and Skaar, E. P. (2011) Nutrient metal sequestration by calprotectin inhibits bacterial superoxide defense, enhancing neutrophil killing of *Staphylococcus aureus*, *Cell Host Microbe 10*, 158-164.
[25] Brophy, M. B., Hayden, J. A., and Nolan, E. M. (2012) Calcium ion gradients modulate the zinc affinity and antibacterial activity of human calprotectin, *J. Am. Chem. Soc. 134*, 18089-18100.
[26] Damo, S. M., Kehl-Fie, T. E., Sugitani, N., Holt, M. E., Rathi, S., Murphy, W. J., Zhang, Y., Betz, C., Hench, L., Fritz, G., Skaar, E. P., and Chazin, W. J. (2013) Molecular basis for manganese sequestration by calprotectin and roles in the innate immune response to invading bacterial pathogens, *Proc. Natl. Acad. Sci. U. S. A. 110*, 3841-3846.
[27] Nakashige, T. G., Stephan, J. R., Cunden, L. S., Brophy, M. B., Wommack, A. J., Keegan, B. C., Shearer, J. M., and Nolan, E. M. (2016) The hexahistidine motif of host-defense protein human calprotectin contributes to zinc withholding and its functional versatility, *J. Am. Chem. Soc. 138*, 12243-12251.
[28] Nakashige, T. G., Zhang, B., Krebs, C., and Nolan, E. M. (2015) Human calprotectin is an iron-sequestering host-defense protein, *Nat. Chem. Biol. 11*, 765-771.
[29] Hayden, J. A., Brophy, M. B., Cunden, L. S., and Nolan, E. M. (2013) High-affinity manganese coordination by human calprotectin is calcium-dependent and requires the histidine-rich site formed at the dimer interface, *J. Am. Chem. Soc. 135*, 775-787.
[30] Nakashige, T. G., Zygiel, E. M., Drennan, C. L., and Nolan, E. M. (2017) Nickel sequestration by the host-defense protein human calprotectin, *J. Am. Chem. Soc. 139*, 8828-8836.
[31] Zygiel, E. M., Nelson, C. E., Brewer, L. K., Oglesby-Sherrouse, A. G., and Nolan, E. M. (2019) The human innate immune protein calprotectin induces iron starvation responses in *Pseudomonas aeruginosa*, *J. Biol. Chem. 294*, 3549-3562.
[32] Brophy, M. B., Nakashige, T. G., Gaillard, A., and Nolan, E. M. (2013) Contributions of the S100A9 C-terminal tail to high-affinity Mn(II) chelation by the host-defense protein human calprotectin, *J. Am. Chem. Soc. 135*, 17804-17817.
[33] Gagnon, D. M., Brophy, M. B., Bowman, S. E. J., Stich, T. A., Drennan, C. L., Britt, R. D., and Nolan, E. M. (2015) Manganese binding properties of human calprotectin under conditions of high and low calcium: X-ray crystallographic and advanced electron paramagnetic resonance spectroscopic analysis, *J. Am. Chem. Soc. 137*, 3004-3016.
[34] Moroz, O. V., Antson, A. A., Grist, S. J., Maitland, N. J., Dodson, G. G., Wilson, K. S., Lukanidin, E., and Bronstein, I. B. (2003) Structure of the human S100A12–copper complex: implications for host-parasite defence, *Acta Crystallogr., Sect. D: Biol. Crystallogr. 59*, 859-867.
[35] Moroz, O. V., Blagova, E. V., Wilkinson, A. J., Wilson, K. S., and Bronstein, I. B. (2009) The crystal structures of human S100A12 in apo form and in complex with zinc: new insights into S100A12 oligomerisation, *J. Mol. Biol. 391*, 536-551.
[36] Cunden, L. S., Gaillard, A., and Nolan, E. M. (2016) Calcium ions tune the zinc-sequestering properties and antimicrobial activity of human S100A12, *Chem. Sci. 7*, 1338-1348.
[37] Baker, T. M., Nakashige, T. G., Nolan, E. M., and Neidig, M. L. (2017) Magnetic circular dichroism studies of iron(II) binding to human calprotectin, *Chem. Sci. 8*, 1369-1377.
[38] Strupat, K., Rogniaux, H., Van Dorsselaer, A., Roth, J., and Vogl, T. (2000) Calcium-induced noncovalently linked tetramers of MRP8 and MRP14 are confirmed by electrospray ionization-mass analysis, *J. Am. Soc. Mass Spectrom. 11*, 780-788.
[39] Teigelkamp, S., Bhardwaj, R. S., Roth, J., Meinardus-Hager, G., Karas, M., and Sorg, C. (1991) Calcium-dependent complex assembly of the myeloic differentiation proteins MRP-8 and MRP-14, *J. Biol. Chem. 266*, 13462-13467.
[40] Hadley, R. C., Gu, Y., and Nolan, E. M. (2018) Initial biochemical and functional evaluation of murine calprotectin reveals Ca(II)-dependence and its ability to chelate multiple nutrient transition metal ions, *Biochemistry 57*, 2846-2856.
[41] Moroz, O. V., Burkitt, W., Wittkowski, H., He, W., Ianoul, A., Novitskaya, V., Xie, J. J., Polyakova, O., Lednev, I. K., Shekhtman, A., Derrick, P. J., Bjoerk, P., Foell, D., and Bronstein, I. B. (2009) Both

Ca^{2+} and Zn^{2+} are essential for S100A12 protein oligomerization and function, *BMC Biochem. 10*, 11.
[42] Wang, Q., Aleshintsev, A., Bolton, D., Zhuang, J., Brenowitz, M., and Gupta, R. (2019) Ca(II) and Zn(II) cooperate to modulate the structure and self-assembly of S100A12, *Biochemistry 58*, 2269-2281.
[43] Matulova, M., Rajova, J., Vlasatikova, L., Volf, J., Stepanova, H., Havlickova, H., Sisak, F., and Rychlik, I. (2012) Characterization of chicken spleen transcriptome after infection with *Salmonella enterica* serovar Enteritidis, *Plos One 7*, e48101.
[44] Rychlik, I., Elsheimer-Matulova, M., and Kyrova, K. (2014) Gene expression in the chicken caecum in response to infections with non-typhoid *Salmonella*, *Vet. Res. 45*, 119.
[45] Sekelova, Z., Stepanova, H., Polansky, O., Varmuzova, K., Faldynova, M., Fedr, R., Rychlik, I., and Vlasatikova, L. (2017) Differential protein expression in chicken macrophages and heterophils in vivo following infection with *Salmonella* Enteritidis, *Vet. Res. 48*, 35.
[46] Matulova, M., Varmuzova, K., Sisak, F., Havlickova, H., Babak, V., Stejskal, K., Zdrahal, Z., and Rychlik, I. (2013) Chicken innate immune response to oral infection with *Salmonella enterica* serovar Enteritidis, *Vet. Res. 44*, 37.
[47] Volf, J., Polansky, O., Varmuzova, K., Gerzova, L., Sekelova, Z., Faldynova, M., Babak, V., Medvecky, M., Smith, A. L., Kaspers, B., Velge, P., and Rychlik, I. (2016) Transient and prolonged response of chicken cecum mucosa to colonization with different gut microbiota, *Plos One 11*, e0163932.
[48] Waterhouse, A., Bertoni, M., Bienert, S., Studer, G., Tauriello, G., Gumienny, R., Heer, F. T., de Beer, T. A. P., Rempfer, C., Bordoli, L., Lepore, R., and Schwede, T. (2018) SWISS-MODEL: homology modelling of protein structures and complexes, *Nucleic Acids Res. 46*, W296-W303.
[49] Chang, C.-C., Khan, I., Tsai, K.-L., Li, H. C., Yang, L.-W., Chou, R.-H., and Yu, C. (2016) Blocking the interaction between S100A9 and RAGE V domain using CHAPS molecule: A novel route to drug development against cell proliferation, *Biochim. Biophys. Acta, Proteins Proteom. 1864*, 1558-1569.
[50] Cunden, L. S., Brophy, M. B., Rodriguez, G. E., Flaxman, H. A., and Nolan, E. M. (2017) Biochemical and functional evaluation of the intramolecular disulfide bonds in the zinc-chelating antimicrobial protein human S100A7 (psoriasin), *Biochemistry 56*, 5726-5738.
[51] Vogl, T., Leukert, N., Barczyk, K., Strupat, K., and Roth, J. (2006) Biophysical characterization of S100A8 and S100A9 in the absence and presence of bivalent cations, *Biochim. Biophys. Acta 1763*, 1298-1306.
[52] Stephan, J. R., and Nolan, E. M. (2016) Calcium-induced tetramerization and zinc chelation shield human calprotectin from degradation by host and bacterial extracellular proteases, *Chem. Sci. 7*, 1962-1975.
[53] Richardson, C. E. R., Cunden, L. S., Butty, V. L., Nolan, E. M., Lippard, S. J., and Shoulders, M. D. (2018) A method for selective depletion of Zn(II) ions from complex biological media and evaluation of cellular consequences of Zn(II) deficiency, *J. Am. Chem. Soc. 140*, 2413-2416.
[54] Stojiljkovic, I., Baumler, A. J., and Heffron, F. (1995) Ethanolamine utilization in *Salmonella typhimurium*: nucleotide sequence, protein expression, and mutational analysis of the *cchA cchB eutE eutJ eutG eutH* gene cluster, *J. Bacteriol. 177*, 1357-1366.
[55] Thomson, N. R., Clayton, D. J., Windhorst, D., Vernikos, G., Davidson, S., Churcher, C., Quail, M. A., Stevens, M., Jones, M. A., Watson, M., Barron, A., Layton, A., Pickard, D., Kingsley, R. A., Bignell, A., Clark, L., Harris, B., Ormond, D., Abdellah, Z., Brooks, K., Cherevach, I., Chillingworth, T., Woodward, J., Norberczak, H., Lord, A., Arrowsmith, C., Jagels, K., Moule, S., Mungall, K., Sanders, M., Whitehead, S., Chabalgoity, J. A., Maskell, D., Humphrey, T., Roberts, M., Barrow, P. A., Dougan, G., and Parkhill, J. (2008) Comparative genome analysis of *Salmonella* Enteritidis PT4 and *Salmonella* Gallinarum 287/91 provides insights into evolutionary and host adaptation pathways, *Genome Res. 18*, 1624-1637.
[56] Maret, W., and Vallee, B. L. (1998) Thiolate ligands in metallothionein confer redox activity on zinc clusters, *Proc. Natl. Acad. Sci. U. S. A. 95*, 3478-3482.
[57] Talmard, C., Bouzan, A., and Faller, P. (2007) Zinc binding to amyloid-beta: Isothermal titration calorimetry and Zn competition experiments with Zn sensors, *Biochemistry 46*, 13658-13666.

[58] Golynskiy, M. V., Gunderson, W. A., Hendrich, M. P., and Cohen, S. M. (2006) Metal binding studies and EPR spectroscopy of the manganese transport regulator MntR, *Biochemistry 45*, 15359-15372.
[59] Simons, T. J. B. (1993) Measurement of free Zn^{2+} ion concentration with the fluorescent-probe Mag-Fura-2 (Furaptra) *J. Biochem. Biophys. Meth. 27*, 25-37.
[60] Burdette, S. C., Frederickson, C. J., Bu, W. M., and Lippard, S. J. (2003) ZP4, an improved neuronal Zn^{2+} sensor of the Zinpyr family, *J. Am. Chem. Soc. 125*, 1778-1787.
[61] Kuzmic, P. (1996) Program DYNAFIT for the analysis of enzyme kinetic data: Application to HIV proteinase, *Anal. Biochem. 237*, 260-273.
[62] Green, L. M., and Berg, J. M. (1989) A retroviral Cys-Xaa_2-Cys-Xaa_4-His-Xaa_4-Cys peptide binds metal ions: Spectroscopic studies and a proposed three-dimensional structure, *Proc. Natl. Acad. Sci. U. S. A. 86*, 4047-4051.
[63] Shi, Y. G., Beger, R. D., and Berg, J. M. (1993) Metal-binding properties of single amino-acid deletion mutants of zinc finger peptides: Studies using cobalt(II) as a spectroscopic probe, *Biophys. J. 64*, 749-753.
[64] Guerrerio, A. L., and Berg, J. M. (2004) Metal ion affinities of the zinc finger domains of the metal responsive element-binding transcription factor-1 (MTF1), *Biochemistry 43*, 5437-5444.
[65] Sivo, V., D'Abrosca, G., Russo, L., Iacovino, R., Pedone, P. V., Fattorusso, R., Isernia, C., and Malgieri, G. (2017) Co(II) coordination in prokaryotic zinc finger domains as revealed by UV-Vis spectroscopy, *Bioinorg. Chem. Appl. 2017,* 1527247.
[66] Nakashige, T. G., Bowman, S. E. J., Zygiel, E. M., Drennan, C. L., and Nolan, E. M. (2018) Biophysical examination of the calcium-modulated nickel-binding properties of human calprotectin reveals conformational change in the EF-hand domains and His_3Asp site, *Biochemistry 57*, 4155-4164.
[67] Korndörfer, I. P., Brueckner, F., and Skerra, A. (2007) The crystal structure of the human $(S100A8/S100A9)_2$ heterotetramer, calprotectin, illustrates how conformational changes of interacting alpha-helices can determine specific association of two EF-hand proteins, *J. Mol. Biol. 370*, 887-898.
[68] Hadley, R. C., Gagnon, D. M., Ozarowski, A., Britt, R. D., and Nolan, E. M. (2019) Murine calprotectin coordinates Mn(II) at a hexahistidine site with Ca(II)-dependent affinity, *Inorg. Chem.58*, 13578-13590.
[69] Gläser, R., Harder, J., Lange, H., Bartels, J., Christophers, E., and Schroder, J.-M. (2005) Antimicrobial psoriasin (S100A7) protects human skin from *Escherichia coli* infection, *Nat. Immunol. 6*, 57-64.
[70] Hein, K. Z., Takahashi, H., Tsumori, T., Yasui, Y., Nanjoh, Y., Toga, T., Wu, Z. H., Grötzinger, J., Jung, S., Wehkamp, J., Schroeder, B. O., Schroeder, J. M., and Morita, E. (2015) Disulphide-reduced psoriasin is a human apoptosis-inducing broad-spectrum fungicide, *Proc. Natl. Acad. Sci. U. S. A. 112*, 13039-13044.